

Cylinder gratings in conical incidence with applications to modes of air-cored photonic crystal fibers

G. H. Smith and L. C. Botten

School of Mathematical Sciences, University of Technology, Sydney, New South Wales 2007, Australia

R. C. McPhedran

School of Physics, University of Sydney, New South Wales 2006, Australia

N. A. Nicorovici

School of Mathematical Sciences, University of Technology, Sydney, New South Wales 2007, Australia

and School of Physics, University of Sydney, New South Wales 2006, Australia

(Received 26 April 2002; published 19 November 2002)

We develop a formulation for cylinder gratings in conical incidence, using a multipole method. The theory, and its numerical implementation, is applied to two-dimensional photonic crystals consisting of a stack of one-dimensional gratings, each characterized by its plane wave scattering matrix. These matrices are used in combination with Bloch's theorem to determine the band structure of the photonic crystal from the solution of an eigenvalue problem. We show that the theory is well adapted to the difficult task of locating the complete band gaps needed to support air-guided modes in microstructured optical fibers, that is, optical fibers in which the confinement of light in a central air hole is achieved by photonic band-gap effects in a periodic cladding comprising a lattice of air holes in a glass matrix.

DOI: 10.1103/PhysRevE.66.056604

PACS number(s): 42.25.Fx, 42.70.Qs, 42.81.Dp, 78.20.Bh

I. INTRODUCTION

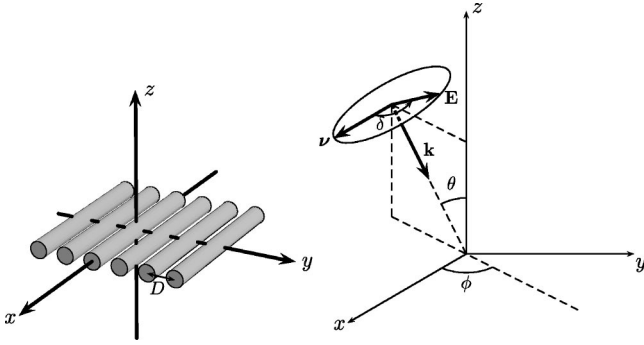
The study of the electromagnetic diffraction by gratings is now a mature field, with numerical formulations available to provide results of high accuracy for theoretical and technological investigations (see, for example, the books by Hutley [1] and by Loewen and Popov [2]). However, by far the majority of investigations into grating diffraction concern themselves with the case of classical diffraction, where the grating is illuminated by a plane wave with a zero component along the direction of the grating generators. Loewen and Popov justify this in the following way: "The more general case of conical diffraction does not introduce fundamental difficulties, but complicates the mathematical and numerical treatment and also is not widely used in practice. Any theory that can deal successfully with the two fundamental cases of polarization can be generalized, if necessary, to deal with the conical case." It is one of the purposes of this paper to show that this judgement was somewhat premature, given two recent applications which have emerged, and which justify the development of formulations for conical diffraction by gratings. Both are connected with photonic band-gap structures. The first is the so-called woodpile structure for achieving a photonic band gap. For references relating to the origin of this geometry, see Ref. [3]. It has attracted much attention recently, since it is a three-dimensional structure, yet it can be fabricated using two-dimensional lithography in a multistep process. As a result, Lin and Fleming [4,5] have been able to fabricate a structure exhibiting a band gap at the important telecommunications wavelength band near 1.5 μm .

The second application is concerned with microstructured optical fibers, a new type of optical fiber in which confinement of light is achieved by the introduction of numerous air

holes running parallel to the fiber rather than by doping the fiber core [6,7]. One type of microstructured optical fiber has a central air hole as well as confining air holes, and its aim is to achieve a fiber in which light propagates as much as possible in air [8–10]. The confinement of light in the central air hole is achieved by photonic band-gap effects and the location of the modes that can propagate in this type of fiber is a numerically difficult task. We will show how this task may be expedited using the scattering properties of gratings in conical incidence.

The diffraction grating we study here is an assemblage of circular cylinders, which may be composed of either dielectric or metal. For simplicity, we will consider the case where the unit cell of the grating contains only one cylinder, although the generalization to multiple cylinders per unit cell is straightforward and valuable [11,12]. We note that Li [13] has treated conical diffraction by gratings composed of rectangular rods, generalizing our earlier work on a modal formulation for dielectric and metallic lamellar gratings [14], while Centeno and Felbacq [15,16] consider the behavior of band gaps in photonic crystals as functions of polarization and conicity of the incident plane wave. Li's formulation has been exploited in recent work on woodpiles composed of dielectric lamellar gratings in the thesis by Gralak [17].

We begin with the formulation for the theory for the conical diffraction of a single cylinder grating (Sec. II). This method extends the treatment of Refs. [18,19] to derive plane wave scattering matrices and, in Sec. III, a different form of the Bloch method, which enables us to compute dispersion diagrams for periodic structures such as photonic crystals. The method is based on a Rayleigh identity treatment [11,12] involving lattice sums, which are in keeping with Maystre's theorem on conical diffraction [20], in that they are the same as lattice sums for classical diffraction if we replace the wave

FIG. 1. A grating of cylinders in the xy plane.

vector by its projection perpendicular to the grating plane. The formulation has been verified using a set of convergence and conservation criteria and by comparison with our previous formulations for classical incidence [18,21]. In Sec. IV, our techniques are applied to the study of the modes which can exist in photonic crystals composed of circular dielectric rods, for the case of out-of-plane propagation [22]. We show that this leads to a method capable of indicating the regions in which one may expect to find the air-guided modes of microstructured optical fibers (MOF) with air cores [8,9].

In a future paper, we shall apply this treatment to structures in the woodpile configuration [3]. The additional layer introduces dispersion in the orthogonal direction and the plane wave set is indexed by dual subscripts. This feature is adopted here to maintain a consistent notation for both papers. The prescription of the scattering matrix requires the solution of a family of diffraction problems (for each layer) associated with the dispersion directions introduced by the second layer. The scattering matrices are thus not dense, but comprise a sequence of blocks (or some permutation thereof), each derived from the application of the basic conical diffraction problem. The theory can then be applied to deduce the spectral properties of the woodpile layering and the band diagram for a woodpile photonic crystal.

We conclude this introductory section with a brief description of our notation. At the lowest level (level 1, say), we denote vectors and matrices by boldface Roman or Greek letters ($\mathbf{A}, \hat{\mathbf{x}}, \delta, \dots$). The notation $\mathbf{f} = [f_s]$ denotes a vector of coefficients f_s . Block matrices of level 1 objects are denoted by boldface calligraphic capital letters or, occasionally, boldface Fraktur capitals ($\mathcal{A}, \mathcal{F}, \mathfrak{R}, \dots$). Such level 2 objects encapsulate both electric and magnetic fields or TE and TM fields. Block matrices of level 2 objects are denoted by bold sans serif capital letters ($\mathbf{S}, \mathbf{F}, \dots$). These encapsulate fields both above and below a grating.

II. CONICAL DIFFRACTION THEORY

A. Outline of the theory

We consider conical diffraction by a single grating consisting of a planar layer of identical parallel cylindrical rods of radius a whose axes are separated by a distance D . In the chosen Cartesian coordinate system, the cylinder axes are parallel to the x axis and lie in the xy plane (Fig. 1). The problem is formulated in terms of the longitudinal compo-

ponents E_x and H_x , for which we develop plane wave expansions in terms of the TE and TM resonates of the electric field (Sec. II B).

In Sec. II C, we make use of the Rayleigh multipole method in which the longitudinal components of the field in the vicinity of the grating are expressed in terms of two-dimensional cylindrical harmonic functions, with field sources represented by the irregular functions (i.e., Hankel functions of the first kind). The essence of the Rayleigh method is that the regular, or nonsingular, part of the field (expressed in terms of Bessel functions of the first kind) in the vicinity of each cylinder derives from sources on all the other cylinders, plus contributions from sources at infinity which appear in the form of incident plane waves. In the case of a grating, the periodicity imposes a Bloch condition on the source coefficients that leads to the introduction of lattice sums that encapsulate the periodicity and geometry of the lattice. In this way, we may determine the coefficients of the source terms associated with each cylinder and subsequently reconstruct the outgoing reflected and transmitted plane wave coefficients (Sec. II D), in turn leading to the computation of plane wave scattering matrices.

For gratings which are up-down symmetric, it is possible to take advantage of the symmetry to reduce the computational complexity of the formulation. In Ref. [18], this simplification was implemented by considering two problems, associated, respectively, with symmetric and antisymmetric incidence field configurations from above and below the grating; an arbitrary problem can always be written as a superposition of these. This enables the resulting systems of equations to be “folded,” thereby halving their number. In this paper we adopt a more general approach by supposing that the grating is illuminated from both above and below with arbitrary incident fields. This enables the diffraction properties of the grating to be characterized by plane wave scattering matrices that specify reflection and transmission coefficients in each output channel (i.e., diffracted order), corresponding to unit inputs in each of these channels (Sec. II D). In this way, we are able to express the scattering matrix as a 2×2 block matrix, in which individual blocks separately comprise reflection and transmission matrices from above and below the grating [Eqs. (52) and (53)]. The advantage of this approach is that no assumptions are made regarding the up-down symmetry of the grating, but in the case where the grating is up-down symmetric, we are still able to reduce the number of equations by a folding procedure.

B. Plane wave expansions

We consider a single grating consisting of identical parallel cylindrical rods of radius a whose axes are separated by a distance D . In the chosen Cartesian coordinate system, the cylinder axes are parallel to the x axis and lie in the xy plane (Fig. 1). The primary incidence channel is defined by the wave vector

$$\mathbf{k}_i = (\alpha_0, \beta_0, -\gamma_0), \quad (1)$$

with wave number $k = \omega/c = (\alpha_0^2 + \beta_0^2 + \gamma_0^2)^{1/2}$, where ω is

the angular frequency and c is the speed of light in vacuum. With θ denoting the angle between \mathbf{k}_i and the z axis, and ϕ denoting the azimuthal angle between the projection of \mathbf{k}_i onto the xy plane and the positive direction of the x axis, the wave-vector components of the specular channel are $\alpha_0 = k \sin \theta \cos \phi$, $\beta_0 = k \sin \theta \sin \phi$, $\gamma_0 = k \cos \theta$.

We denote the transverse resolute in the xy plane of field quantities by a subscripted t (e.g., \mathbf{E}_t), while scalar components along the x , y , and z axes will be denoted by E_x , E_y , and E_z , respectively. We introduce $\mathbf{K} = Z_0 \mathbf{H}$, where $Z_0 = \sqrt{\mu_0 / \epsilon_0}$ is the characteristic impedance of free space, thus normalizing the field equations to involve only electric quantities.

We resolve the fields into a sum of two principal polarizations: transverse magnetic (TM), in which $\mathbf{K} = \mathbf{K}_t$, and transverse electric (TE), in which $\mathbf{E} = \mathbf{E}_t$. These modes are specified by a polarization angle δ (Fig. 1), which is the angle between the direction of the electric field \mathbf{E} and the vector

$$\boldsymbol{\nu} = \frac{\mathbf{k}_i \times \hat{\mathbf{z}}}{k \sin \theta} \quad (2)$$

normal to the plane of incidence. For TE and TM polarizations, we have $\delta = 0, \pi/2$, respectively.

The periodicity of the layer of cylinders introduces dispersion in the y direction characterized by $e^{i\beta_p y}$, with $\beta_p = \beta_0 + 2\pi p/D$. For in-plane incidence in either of the two principal polarizations, the problem is x invariant for a single layer. However, in conical diffraction, the x dependence is $e^{i\alpha_q x}$ while the addition of orthogonal layers, as in a woodpile, introduces dispersion in the x direction, leading to an x dependence of $e^{i\alpha_q x}$, with $\alpha_q = \alpha_0 + 2\pi q/D$. The formulation of the single-layer scattering matrices for a two-dimensional (2D) diffraction problem in such configurations thus requires the solution of the family $\{q\}$ of diffraction problems associated with all possible α_q directions. For convenience, we index plane wave coefficients by s , which denotes the pair (p, q) for crossed orthogonal gratings, or the simple subscript p [more precisely $(p, 0)$] for conical diffraction involving only one-dimensional grating structures, or stacks of such. If we put $\mathbf{Q}_s = \alpha_q \hat{\mathbf{x}} + \beta_p \hat{\mathbf{y}}$, the z dependence of plane wave fields may be written as $e^{\pm i\gamma_s z}$, where

$$\gamma_s = \sqrt{k^2 - Q_s^2}, \quad s \in \Omega_r = \{s | Q_s^2 < k^2\} \quad (3)$$

$$\gamma_s = i\sqrt{Q_s^2 - k^2}, \quad s \in \Omega_e = \{s | Q_s^2 > k^2\}, \quad (4)$$

with $s = (p, q)$ denoting an integer pair.

As in Ref. [23], we expand the transverse fields in linear combinations of the TE and TM plane wave modes,

$$\mathbf{R}_s^M(\mathbf{r}) = \frac{\mathbf{Q}_s}{Q_s} e^{i\mathbf{Q}_s \cdot \mathbf{r}}, \quad \mathbf{R}_s^E(\mathbf{r}) = \frac{\hat{\mathbf{z}} \times \mathbf{Q}_s}{Q_s} e^{i\mathbf{Q}_s \cdot \mathbf{r}}. \quad (5)$$

We define $\xi_s = \gamma_s/k$. Above the grating [23], the transverse electric and magnetic fields are

$$\begin{aligned} \mathbf{E}_t = & \sum_s [\xi_s^{-1/2} \{E_{I,s}^- e^{-i\gamma_s z} + E_{D,s}^+ e^{i\gamma_s z}\} \mathbf{R}_s^E \\ & + \xi_s^{1/2} \{F_{I,s}^- e^{-i\gamma_s z} + F_{D,s}^+ e^{i\gamma_s z}\} \mathbf{R}_s^M], \end{aligned} \quad (6)$$

$$\begin{aligned} \hat{\mathbf{z}} \times \mathbf{K}_t = & \sum_s [\xi_s^{1/2} \{E_{I,s}^- e^{-i\gamma_s z} - E_{D,s}^+ e^{i\gamma_s z}\} \mathbf{R}_s^E \\ & + \xi_s^{-1/2} \{F_{I,s}^- e^{-i\gamma_s z} - F_{D,s}^+ e^{i\gamma_s z}\} \mathbf{R}_s^M], \end{aligned} \quad (7)$$

where $E_{I,s}^-$ and $F_{I,s}^-$, respectively, denote the TE and TM components of the incoming electric field, while $E_{D,s}^+$ and $F_{D,s}^+$, respectively, denote the TE and TM components of the outgoing electric field in the upper half space. In the half space below the grid, there exist analogous expressions for \mathbf{E}_t and $\hat{\mathbf{z}} \times \mathbf{E}_t$ in terms of the components $E_{I,s}^+$ and $F_{I,s}^+$ of the incoming electric field and the components $E_{D,s}^-$ and $F_{D,s}^-$ of the outgoing electric field.

While the plane wave diffraction problem is best formulated in TE/TM modes, the multipole scattering problem is best handled in terms of principal Cartesian field components parallel to the cylinder axes. These may be derived from Eqs. (6) and (7), using $E_x = \mathbf{E}_t \cdot \hat{\mathbf{x}}$ and $K_x = -\hat{\mathbf{z}} \times (\hat{\mathbf{z}} \times \mathbf{K}_t) \cdot \hat{\mathbf{x}}$. This leads to

$$\begin{bmatrix} E_x \\ K_x \end{bmatrix} = \sum_s \left\{ \begin{bmatrix} \delta_{E,s}^- \\ \delta_{K,s}^- \end{bmatrix} e^{-i\gamma_s z} + \begin{bmatrix} f_{E,s}^+ \\ f_{K,s}^+ \end{bmatrix} e^{i\gamma_s z} \right\} e^{i\mathbf{Q}_s \cdot \mathbf{r}} \quad (8)$$

above the grating and

$$\begin{bmatrix} E_x \\ K_x \end{bmatrix} = \sum_s \left\{ \begin{bmatrix} f_{E,s}^- \\ f_{K,s}^- \end{bmatrix} e^{-i\gamma_s z} + \begin{bmatrix} \delta_{E,s}^+ \\ \delta_{K,s}^+ \end{bmatrix} e^{i\gamma_s z} \right\} e^{i\mathbf{Q}_s \cdot \mathbf{r}} \quad (9)$$

below the grating, where the outgoing fields $[f_{E,s}^\pm]$ and $[f_{K,s}^\pm]$ are defined by

$$\begin{bmatrix} f_{E,s}^+ \\ f_{K,s}^+ \end{bmatrix} = \begin{bmatrix} -\xi_\beta & \xi_\alpha \\ -\xi_\alpha & -\xi_\beta \end{bmatrix} \begin{bmatrix} E_{D,s}^+ \\ F_{D,s}^+ \end{bmatrix}, \quad (10)$$

$$\begin{bmatrix} f_{E,s}^- \\ f_{K,s}^- \end{bmatrix} = \begin{bmatrix} -\xi_\beta & \xi_\alpha \\ \xi_\alpha & \xi_\beta \end{bmatrix} \begin{bmatrix} E_{D,s}^- \\ F_{D,s}^- \end{bmatrix} \quad (11)$$

and where

$$\xi_\beta = [\xi_s^{-1/2} \beta_p / Q_s], \quad \xi_\alpha = [\xi_s^{1/2} \alpha_q / Q_s]. \quad (12)$$

The incoming fields $[\delta_{E,s}^\pm]$ and $[\delta_{K,s}^\pm]$ are defined analogously to $[f_{E,s}^\pm]$ and $[f_{K,s}^\pm]$.

C. Multipole expansions

Here, we consider conical diffraction of fields with a specified x dependence of $e^{i\alpha_q x}$, and form a 2D projection of the problem in the yz plane, denoting $\mathbf{r} = (y, z)$ (Fig. 2). Then,

$$\nabla_{yz}^2 \mathbf{E} + k_\perp^2 \mathbf{E} = 0,$$

$$\nabla_{yz}^2 \mathbf{H} + k_\perp^2 \mathbf{H} = 0,$$

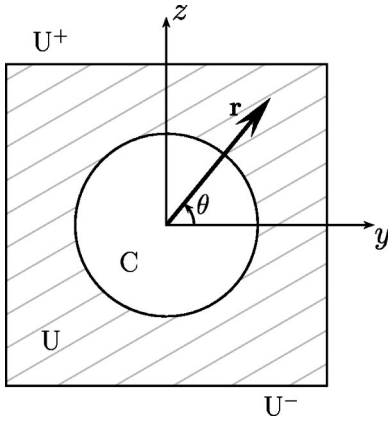


FIG. 2. The unit cell for a single-layer grating. The crosshatched region represents the area $U \setminus C$ for the first integral in Green's theorem [Eq. (19)].

where the projected wave vector k_{\perp} is given by $k_{\perp}^2 + \alpha_q^2 = k^2$ and ∇_{yz}^2 denotes the operator $\partial^2/\partial y^2 + \partial^2/\partial z^2$. We introduce the free space Green's function G , possessing the quasiperiodicity of the incident field and satisfying

$$(\nabla_{yz}^2 + k_{\perp}^2)G(\mathbf{r}) = \sum_{n=-\infty}^{\infty} \delta(\mathbf{r} - nD\hat{\mathbf{x}})e^{i\beta_0 nD}. \quad (13)$$

Its Cartesian representation is

$$G(\mathbf{r}) = \frac{1}{2iD} \sum_{p=-\infty}^{\infty} \frac{1}{\gamma_s} e^{i(\beta_p y + \gamma_s |z|)}, \quad (14)$$

while in the cylindrical harmonic form, the Green's function is

$$G(\mathbf{r}) = -\frac{i}{4} \left[H_0^{(1)}(k_{\perp}|\mathbf{r}|) + \sum_{m=-\infty}^{\infty} S_m J_m(k_{\perp}|\mathbf{r}|) e^{-im \arg(\mathbf{r})} \right], \quad (15)$$

where $\arg(\mathbf{r})$ denotes the polar angle of the vector \mathbf{r} . This form (15) of the Green's function [24–27] underpins the application of the Rayleigh method and mirrors the structure of the field identity. Its first term, having a singularity (or source) at the origin, is associated with a contribution from the central ($n=0$) unit cell, while the other terms, associated with the regular Bessel functions, derive from sources in all other unit cells ($n \neq 0$), with contributions specified by the lattice sums

$$S_m = \sum_{n \neq 0} H_m^{(1)}(|n|k_{\perp}D) e^{i\beta_0 nD} e^{im\varphi_n}. \quad (16)$$

Here, $\varphi_n = \pi\mathcal{H}(-n)$, where \mathcal{H} is the usual Heaviside step function.

The longitudinal field components in the vicinity of each cylinder may be written in terms of cylindrical harmonics with the following representations:

$$E_x(r, \theta) = \sum_{n=-\infty}^{\infty} [A_n^E J_n(k_{\perp}r) + B_n^E H_n^{(1)}(k_{\perp}r)] e^{in\theta} e^{i\alpha_q x}, \quad (17)$$

$$K_x(r, \theta) = \sum_{n=-\infty}^{\infty} [A_n^K J_n(k_{\perp}r) + B_n^K H_n^{(1)}(k_{\perp}r)] e^{in\theta} e^{i\alpha_q x}, \quad (18)$$

applying in the vicinity of the central cylinder. In all other cells, the field is inferred from the Bloch condition which, in turn, implies that the coefficients for the field expansions in cell m satisfy a quasiperiodicity relation $B_n^{(m)} = B_n \exp(im\beta_0 D)$.

As illustrated in Fig. 2, the region C is the cross section of the cylinder inside the unit cell U and we let $A = U \setminus C$ denote the area enclosed by the perimeter of the cylinder and the boundary of the unit cell. The boundary of A is denoted ∂A . The multipole coefficients $\mathbf{B}^E = [B_n^E]$ and $\mathbf{B}^K = [B_n^K]$ may now be determined from a Rayleigh field identity, the derivation of which follows from Green's theorem,

$$\begin{aligned} E_x(\mathbf{r}) &= \int_A [E_x(\mathbf{r}') \nabla_{\mathbf{r}'}^2 G(\mathbf{r}; \mathbf{r}') - G(\mathbf{r}; \mathbf{r}') \nabla_{\mathbf{r}'}^2 E_x(\mathbf{r}')] dA' \\ &= \oint_{\partial A} \left[E_x(\mathbf{r}') \frac{\partial}{\partial n'} G(\mathbf{r}; \mathbf{r}') - G(\mathbf{r}; \mathbf{r}') \frac{\partial}{\partial n'} E_x(\mathbf{r}') \right] ds', \end{aligned} \quad (19)$$

where n' denotes the outward pointing normal.

Following the treatment in Ref. [18], the Rayleigh identity

$$A_n^E = \sum_{m=-\infty}^{\infty} S_{n-m} B_m^E + \sum_{p=-\infty}^{\infty} (J_{np}^- \delta_{E,p}^- + J_{np}^+ \delta_{E,p}^+) \quad (20)$$

is derived by a straightforward but lengthy manipulation, in which the cylindrical harmonic field representation (17) and the plane wave representations (8) and (9) of fields above and below the grating are substituted into Eq. (19), and the resultant form compared with Eq. (17). In Eq. (20), the first series expresses the contributions to the regular field due to outgoing fields sourced on all other cylinders and depends only on the geometry and periodicity of the grating lattice. The second series arises from contributions due to incoming plane waves from above and below the grating with the J_n^- and J_n^+ , which are given below, respectively, denoting the coefficients of downward and upward propagating incident plane waves in the cylindrical harmonic basis. Here

$$J_{np}^- = (-1)^n e^{-in\vartheta_p}, \quad J_{np}^+ = e^{in\vartheta_p}, \quad (21)$$

where $\vartheta_p = \arg(\beta_p + i\gamma_p)$.

Similarly, we may use Green's theorem to obtain the magnetic field K_x , leading to an analog of Eq. (20). Equation (20) and its magnetic analog may be combined in matrix form to obtain

$$\mathcal{A} = \mathcal{S}\mathcal{B} + \mathcal{J}^{-1} \begin{bmatrix} \delta_E^- \\ \delta_K^- \end{bmatrix} + \mathcal{J}^+ \begin{bmatrix} \delta_E^+ \\ \delta_K^+ \end{bmatrix}, \quad (22)$$

where $\mathcal{A}=[(A^E)^T(A^K)^T]^T$, $\mathcal{B}=[(B^E)^T(B^K)^T]^T$ and

$$\mathcal{S}=\begin{bmatrix} \mathbf{S} & \mathbf{0} \\ \mathbf{0} & \mathbf{S} \end{bmatrix}, \quad \mathbf{S}=[S_{n-m}], \quad \mathcal{J}^\pm=\begin{bmatrix} \mathbf{J}^\pm & \mathbf{0} \\ \mathbf{0} & \mathbf{J}^\pm \end{bmatrix}, \quad (23)$$

with $\mathbf{J}^\pm=[J_{ns}^\pm]$.

The boundary conditions, which require the continuity of the tangential field components (i.e., E_z , K_z , E_θ , and K_θ) at the cylinder boundaries, couple the coefficients A_n^E , A_n^K , B_n^E , and B_n^K through the following equation [derived in Appendix A as Eq. (A14)]:

$$\begin{bmatrix} A_n^E \\ A_n^K \end{bmatrix} = - \begin{bmatrix} M_n^{EE} & M_n^{EK} \\ M_n^{KE} & M_n^{KK} \end{bmatrix} \begin{bmatrix} B_n^E \\ B_n^K \end{bmatrix}, \quad (24)$$

where the matrix elements $M_n^{EE}, M_n^{EK}, M_n^{KE}, M_n^{KK}$ encapsulate the material properties (i.e., refractive indices and radii) of the cylinders. In block matrix form, we write

$$\mathcal{A} = -\mathcal{M}\mathcal{B}, \quad (25)$$

where \mathcal{M} is the block matrix.

$$\mathcal{M} = \begin{bmatrix} \mathbf{M}^{EE} & \mathbf{M}^{EK} \\ \mathbf{M}^{KE} & \mathbf{M}^{KK} \end{bmatrix}. \quad (26)$$

Here $\mathbf{M}^{PQ} = \text{diag}[M_n^{PQ}]$, where P and Q select the polarization parameters E or K .

From Eqs. (22) and (25) we deduce the Rayleigh Identity

$$\mathcal{B} = -(\mathcal{M} + \mathcal{S})^{-1} \left(\mathcal{J}^- \begin{bmatrix} \delta_E^- \\ \delta_K^- \end{bmatrix} + \mathcal{J}^+ \begin{bmatrix} \delta_E^+ \\ \delta_K^+ \end{bmatrix} \right), \quad (27)$$

a linear system for the multipole coefficients \mathcal{B} .

D. Plane wave reconstruction and scattering matrices

Following Appendix C in Ref. [18], the plane wave coefficients $f_{E/K}^\pm$ in Eqs. (8) and (9) may be generated with the aid of Green's theorem (19), where, this time, we exploit the plane wave form (14) of the Green's function and take \mathbf{r} to be located above or below the grating; that is, $z \geq a$ or $z \leq -a$. The reconstruction equation for $f_{E,s}^\pm$ is

$$f_{E,s}^\pm = \delta_{E,s}^\pm + \frac{2}{\gamma_s D} \sum_{n=-\infty}^{\infty} (\pm 1)^n e^{\mp i n \vartheta_s} B_n^E. \quad (28)$$

Equation (28), together with an analogous expression for $f_{K,s}^\pm$ may be cast in matrix form as

$$\begin{bmatrix} \mathcal{F}^- \\ \mathcal{F}^+ \end{bmatrix} = \begin{bmatrix} \mathcal{D}^- \\ \mathcal{D}^+ \end{bmatrix} + \frac{2}{D} \begin{bmatrix} \mathcal{G}^{-1} & \mathbf{0} \\ \mathbf{0} & \mathcal{G}^{-1} \end{bmatrix} \begin{bmatrix} \mathcal{K}^- \\ \mathcal{K}^+ \end{bmatrix} \mathcal{B}, \quad (29)$$

where

$$\mathcal{F}^\pm = \begin{bmatrix} \mathbf{f}_E^\pm \\ \mathbf{f}_K^\pm \end{bmatrix}, \quad \mathcal{D}^\pm = \begin{bmatrix} \delta_E^\pm \\ \delta_E^\pm \end{bmatrix}, \quad (30)$$

$$\mathcal{G} = \begin{bmatrix} \mathbf{G} & \mathbf{0} \\ \mathbf{0} & \mathbf{G} \end{bmatrix}, \quad \mathcal{K}^\pm = \begin{bmatrix} \mathbf{K}^\pm & \mathbf{0} \\ \mathbf{0} & \mathbf{K}^\pm \end{bmatrix}, \quad (31)$$

and where $\mathbf{G} = \text{diag}[\gamma_s]$, $\mathbf{K}^\pm = [K_{sn}^\pm] = [(\pm 1)^n e^{\mp i n \theta_s}]$.

As noted in Sec. II A, it is advantageous to exploit up-down symmetry when it occurs. We do this through the introduction of the *symmetrizing transformation* \mathbf{C} ,

$$\mathbf{C} = \begin{bmatrix} \mathbf{C}^s & \mathbf{C}^a \\ \mathbf{C}^s & -\mathbf{C}^a \end{bmatrix}, \quad (32)$$

where

$$\mathbf{C}^s = \begin{bmatrix} \mathbf{I} & \mathbf{0} \\ \mathbf{0} & \mathbf{I} \end{bmatrix}, \quad \mathbf{C}^a = \begin{bmatrix} \mathbf{I} & \mathbf{0} \\ \mathbf{0} & -\mathbf{I} \end{bmatrix}. \quad (33)$$

(Here, and in the sequel, we use \mathbf{I} , \mathcal{I} , or \mathbf{I} to denote the identity matrix, with the notation determined by the context.) The form of \mathbf{C} reflects the symmetry relationships between electric and magnetic quantities that are imposed by Maxwell's equations. If E_x is symmetric, then H_x is antisymmetric and conversely.

We now develop an expression for the scattering matrix \mathcal{S} , which characterizes the scattered fields above and below the grating. The scattering matrix appears as a 2×2 block matrix, in which the individual partitions separately comprise reflection and transmission matrices from above and below the grating. We begin by multiplying Eq. (29) by \mathbf{C} , which commutes with \mathbf{G} , to form

$$\mathbf{C}\mathcal{F} = \mathbf{C}\mathcal{D} + \frac{2}{D} \mathbf{G}^{-1} \begin{bmatrix} \mathcal{K}^s \\ \mathcal{K}^a \end{bmatrix} \mathcal{B}, \quad (34)$$

where

$$\mathbf{F} = \begin{bmatrix} \mathcal{F}^- \\ \mathcal{F}^+ \end{bmatrix}, \quad \mathbf{D} = \begin{bmatrix} \mathcal{D}^- \\ \mathcal{D}^+ \end{bmatrix}, \quad \mathbf{G} = \begin{bmatrix} \mathcal{G} & \mathbf{0} \\ \mathbf{0} & \mathcal{G} \end{bmatrix},$$

$$\mathcal{K}^s = \begin{bmatrix} \mathbf{K}^\oplus & \mathbf{0} \\ \mathbf{0} & \mathbf{K}^\ominus \end{bmatrix}, \quad \mathcal{K}^a = \begin{bmatrix} \mathbf{K}^\ominus & \mathbf{0} \\ \mathbf{0} & \mathbf{K}^\oplus \end{bmatrix}, \quad (35)$$

and $\mathbf{K}^{\oplus/\ominus} = \mathbf{K}^- \pm \mathbf{K}^+$.

Then, substituting the solution of the Rayleigh identity (27) into Eq. (34) gives

$$\mathbf{C}\mathcal{F} = \mathbf{C}\mathcal{D} - \frac{2}{D} \mathbf{G}^{-1} \begin{bmatrix} \mathcal{K}^s \\ \mathcal{K}^a \end{bmatrix} (\mathcal{M} + \mathcal{S})^{-1} [\mathcal{J}^- \quad \mathcal{J}^+] \mathcal{D}, \quad (36)$$

which we can write as

$$\mathbf{C}\mathcal{F} = \mathbf{C}\mathcal{D} - \frac{2}{D} \mathbf{G}^{-1} \begin{bmatrix} \mathcal{K}^s \mathcal{L} \mathcal{J}^s & \mathcal{K}^s \mathcal{L} \mathcal{J}^a \\ \mathcal{K}^a \mathcal{L} \mathcal{J}^s & \mathcal{K}^a \mathcal{L} \mathcal{J}^a \end{bmatrix} \mathbf{C}\mathcal{D}, \quad (37)$$

where

$$\mathcal{L} = (\mathcal{M} + \mathcal{S})^{-1}, \quad \mathcal{J}^s = \begin{bmatrix} \mathbf{J}^\oplus & \mathbf{0} \\ \mathbf{0} & \mathbf{J}^\ominus \end{bmatrix}, \quad \mathcal{J}^a = \begin{bmatrix} \mathbf{J}^\ominus & \mathbf{0} \\ \mathbf{0} & \mathbf{J}^\oplus \end{bmatrix}, \quad (38)$$

and $\mathbf{J}^{\oplus/\ominus} = \mathbf{J}^- \pm \mathbf{J}^+$.

Equation (37) has been derived without making any assumptions about the symmetry of the grating. However, as shown in Appendix B, the terms $\mathcal{K}^s \mathcal{L} \mathcal{J}^a$ and $\mathcal{K}^a \mathcal{L} \mathcal{J}^s$ vanish for gratings having an up-down symmetry, in which case the system decouples completely.

Next, we express the solution of the diffraction problem in terms of plane wave scattering matrices using TE-TM decompositions of plane wave fields by introducing a transformation that converts the plane wave components contained within \mathbf{F} and \mathbf{D} into TE and TM components. This is done with a transformation \mathcal{X} , whose form follows from Eq. (11). We express \mathcal{X} as the block matrix

$$\mathcal{X} = \begin{bmatrix} -\xi_\beta & \xi_\alpha \\ \xi_\alpha & \xi_\beta \end{bmatrix}, \quad (39)$$

with

$$\xi_\beta = \text{diag} \left[\frac{\xi_s^{-1/2} \beta_q}{Q_s} \right], \quad \xi_\alpha = \text{diag} \left[\frac{\xi_s^{1/2} \alpha_p}{Q_s} \right]. \quad (40)$$

We have

$$\mathbf{C}\mathbf{F} = \begin{bmatrix} \mathcal{X} & \mathbf{0} \\ \mathbf{0} & \mathcal{X} \end{bmatrix} \begin{bmatrix} \mathcal{F}_D^s \\ \mathcal{F}_D^a \end{bmatrix}, \quad \mathbf{C}\mathbf{D} = \begin{bmatrix} \mathcal{X} & \mathbf{0} \\ \mathbf{0} & \mathcal{X} \end{bmatrix} \begin{bmatrix} \mathcal{F}_I^s \\ \mathcal{F}_I^a \end{bmatrix}, \quad (41)$$

where

$$\mathcal{F}_D^s = \begin{bmatrix} \mathbf{E}_D^- + \mathbf{E}_D^+ \\ \mathbf{F}_D^- + \mathbf{F}_D^+ \end{bmatrix}, \quad \mathcal{F}_D^a = \begin{bmatrix} \mathbf{E}_D^- - \mathbf{E}_D^+ \\ \mathbf{F}_D^- - \mathbf{F}_D^+ \end{bmatrix} \quad (42)$$

$$\mathcal{F}_I^s = \begin{bmatrix} \mathbf{E}_I^- + \mathbf{E}_I^+ \\ \mathbf{F}_I^- + \mathbf{F}_I^+ \end{bmatrix}, \quad \mathcal{F}_I^a = \begin{bmatrix} \mathbf{E}_I^- - \mathbf{E}_I^+ \\ \mathbf{F}_I^- - \mathbf{F}_I^+ \end{bmatrix}. \quad (43)$$

We define the scattering matrix \mathbf{S} as

$$\begin{bmatrix} \mathcal{F}_D^s \\ \mathcal{F}_D^a \end{bmatrix} = \mathbf{S} \begin{bmatrix} \mathcal{F}_I^s \\ \mathcal{F}_I^a \end{bmatrix}, \quad (44)$$

so that from Eqs. (37), (41), and (44),

$$\mathbf{S} = \mathbf{I} - \frac{1}{D} \mathbf{X}^{-1} \mathbf{G}^{-1} \begin{bmatrix} \mathcal{K}^s \mathcal{L} \mathcal{J}^s & \mathcal{K}^s \mathcal{L} \mathcal{J}^a \\ \mathcal{K}^a \mathcal{L} \mathcal{J}^s & \mathcal{K}^a \mathcal{L} \mathcal{J}^a \end{bmatrix} \mathbf{X}, \quad (45)$$

where $\mathbf{X} = \text{diag}[\mathcal{X}, \mathcal{X}]$. However, we can express Eq. (45) in a simpler form. It is elementary that $\mathcal{X}^{-1} = \mathcal{L}\mathcal{X}$, where $\mathcal{L} = \text{diag}[(\xi_\alpha^2 + \xi_\beta^2)^{-1}, (\xi_\alpha^2 + \xi_\beta^2)^{-1}]$ and, consequently,

$$\mathcal{X}^{-1} \mathbf{G}^{-1} = \mathcal{L} \mathbf{G}^{-1} \mathcal{X}. \quad (46)$$

A simple calculation shows that the diagonal terms of the matrix $\mathcal{L} \mathbf{G}^{-1}$ are of the form k/k_\perp^2 , so that

$$\mathbf{X}^{-1} \mathbf{G}^{-1} = \frac{k}{k_\perp^2} \mathbf{X}. \quad (47)$$

The scattering matrix \mathbf{S} , in terms of the symmetric and anti-symmetric fields problems, can now be written as

$$\mathbf{S} = \mathbf{I} - \frac{k}{k_\perp^2 D} \mathbf{X} \begin{bmatrix} \mathcal{K}^s \mathcal{L} \mathcal{J}^s & \mathcal{K}^s \mathcal{L} \mathcal{J}^a \\ \mathcal{K}^a \mathcal{L} \mathcal{J}^s & \mathcal{K}^a \mathcal{L} \mathcal{J}^a \end{bmatrix} \mathbf{X}. \quad (48)$$

The final step is to derive terms for the reflection and transmission matrices, using Eq. (48). Using the transformation

$$\mathbf{T} = \begin{bmatrix} \mathcal{I} & \mathcal{I} \\ \mathcal{I} & -\mathcal{I} \end{bmatrix}, \quad (49)$$

we convert the symmetrized field vectors to up and down propagating plane waves as follows:

$$\begin{bmatrix} \mathcal{F}_D^- \\ \mathcal{F}_D^+ \end{bmatrix} = \mathbf{T}^{-1} \begin{bmatrix} \mathcal{F}_D^s \\ \mathcal{F}_D^a \end{bmatrix}, \quad \begin{bmatrix} \mathcal{F}_I^- \\ \mathcal{F}_I^+ \end{bmatrix} = \mathbf{T}^{-1} \begin{bmatrix} \mathcal{F}_I^s \\ \mathcal{F}_I^a \end{bmatrix}, \quad (50)$$

where

$$\mathcal{F}_D^\pm = \begin{bmatrix} \mathbf{E}_D^\pm \\ \mathbf{F}_D^\pm \end{bmatrix}, \quad \mathcal{F}_I^\pm = \begin{bmatrix} \mathbf{E}_I^\pm \\ \mathbf{F}_I^\pm \end{bmatrix}. \quad (51)$$

Consequently,

$$\begin{bmatrix} \mathcal{F}_D^- \\ \mathcal{F}_D^+ \end{bmatrix} = \mathbf{T}^{-1} \mathbf{S} \mathbf{T} \begin{bmatrix} \mathcal{F}_I^- \\ \mathcal{F}_I^+ \end{bmatrix}. \quad (52)$$

Let \mathcal{R}_a and \mathcal{R}_b , respectively, denote reflection matrices for incidence above and below the grating and let \mathcal{T}_a and \mathcal{T}_b denote the corresponding transmission matrices. It is clear that

$$\begin{bmatrix} \mathcal{F}_D^- \\ \mathcal{F}_D^+ \end{bmatrix} = \begin{bmatrix} \mathcal{T}_a & \mathcal{R}_b \\ \mathcal{R}_a & \mathcal{T}_b \end{bmatrix} \begin{bmatrix} \mathcal{F}_I^- \\ \mathcal{F}_I^+ \end{bmatrix}. \quad (53)$$

A comparison between Eqs. (52) and (53) thus yields explicit expressions for the reflection and transmission matrices. In the case where the matrix is up-down symmetric, we have

$$\mathcal{R}_a = \mathcal{R}_b = -\frac{k}{2k_\perp^2 D} \mathcal{X} (\mathcal{K}^s \mathcal{L} \mathcal{J}^s - \mathcal{K}^a \mathcal{L} \mathcal{J}^a) \mathcal{X}, \quad (54)$$

$$\mathcal{T}_a = \mathcal{T}_b = \mathcal{I} - \frac{k}{2k_\perp^2 D} \mathcal{X} (\mathcal{K}^s \mathcal{L} \mathcal{J}^s + \mathcal{K}^a \mathcal{L} \mathcal{J}^a) \mathcal{X}, \quad (55)$$

which generalizes our earlier results in Ref. [18]. For gratings exhibiting up-down symmetry, it is possible to take advantage of various symmetry relationships among the terms in order to halve the number of equations, thus reducing computational complexity. This is discussed in Appendix B.

III. THE BLOCH METHOD

We now lay the groundwork for the consideration of modes in MOFs with air cores in Sec. IV. The same ideas will apply to band diagrams for woodpile configurations. The idea is to use scattering matrices to determine frequency regions in which propagating modes satisfying the Bloch condition exist, and to formulate this condition as an eigenvalue constraint problem, which enables us to determine the band structure of planar, stratified photonic crystals. Our treatment is based on a technique developed originally in electron diffraction by McRae [28] and applied recently in photonic crystals by Gralak [17] and Botten *et al.* [19], but reformulated here to increase the robustness of the method in order to handle the greater computational demands associated with gratings and grids in conical diffraction.

Our earlier approach [19], based upon a \mathbf{T} matrix formulation,¹ worked well for general 2D structures provided that the dimension of the scattering matrices was not too large. To improve the stability of the method for 2D structures, and to make possible the calculations for 3D structures (such as the woodpile), in which the diffracting element generates a doubly dimensioned set of plane waves, we have reformulated the eigenvalue problem in terms of an \mathbf{R} matrix formulation [29,30]. The formulation outlined here applies to the most general (3D) configuration. In the case of the air-guided modes of photonic crystal fibers, a minor simplification, requiring the replacement of a doubly dimensioned set of plane waves by the singly dimensioned set for a grating in conical incidence, is required.

We begin with TE-TM reflection and transmission scattering matrices for the elementary, single layer relative to the standard phase origin at the center of the primary cylinder, and denoted by the superscripted (0). For incidence from above and below, these are $(\mathcal{R}_a^{(0)}, \mathcal{T}_a^{(0)})$ and $(\mathcal{R}_b^{(0)}, \mathcal{T}_b^{(0)})$, respectively. The array is constructed in the yz plane, using basis vectors $\boldsymbol{\sigma} = D\hat{\mathbf{e}}_y$ and $\boldsymbol{\tau} = s_y\hat{\mathbf{e}}_y + s_z\hat{\mathbf{e}}_z$, where s_y and s_z are real. As in Ref. [19], we introduce phase origins at the center of the upper and lower edges of the basic (parallelepiped) cell generated by the basis vectors $\boldsymbol{\sigma}$ and $\boldsymbol{\tau}$ at points $P_1 = (0, s_y/2, s_z/2)$ above the layer and $P_2 = (0, -s_y/2, -s_z/2)$ below the layer (Fig. 3).

Relative to these origins, the component of the electric field transverse to the elementary layer is

$$\mathbf{E}_t^{(j)} = \sum_s [\xi_s^{-1/2} \{E_{j,s}^- e^{-i\gamma_s(z-z_j)} + E_{j,s}^+ e^{i\gamma_s(z-z_j)}\} \mathbf{R}_s^E + \xi_s^{1/2} \{F_{j,s}^- e^{-i\gamma_s(z-z_j)} + F_{j,s}^+ e^{i\gamma_s(z-z_j)}\} \mathbf{R}_s^M], \quad (56)$$

where $j=1$ refers to the region above the layer and $j=2$ to the region below. An analogous expression may be derived from Eq. (7) for the magnetic field. Correspondingly, the reflection and transmission scattering matrices relative to these phase origins are then given by

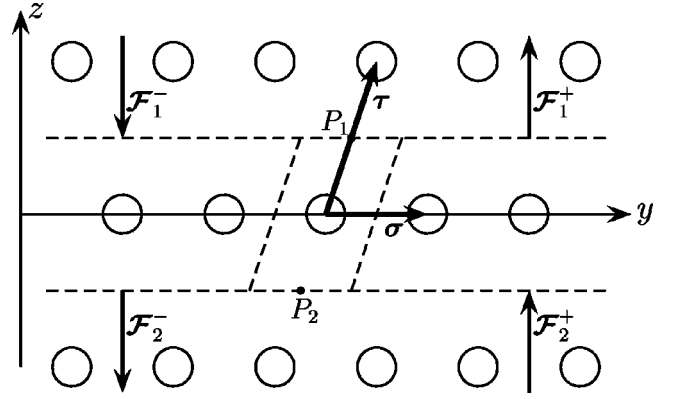


FIG. 3. Geometry of the unit cell (defined by the fundamental translation vectors $\boldsymbol{\sigma}$ and $\boldsymbol{\tau}$) for the Bloch method calculations. The phase origins P_1 and P_2 of the fields \mathcal{F}_1^+ , \mathcal{F}_1^- , \mathcal{F}_2^+ , and \mathcal{F}_2^- , above and below the grating, respectively, are shown.

$$\begin{bmatrix} \mathcal{T}_a & \mathcal{R}_b \\ \mathcal{R}_a & \mathcal{T}_b \end{bmatrix} = \mathbf{Q}\mathbf{P} \begin{bmatrix} \mathcal{T}_a^{(0)} & \mathcal{R}_b^{(0)} \\ \mathcal{R}_a^{(0)} & \mathcal{T}_b^{(0)} \end{bmatrix} \mathbf{P}\mathbf{Q}, \quad (57)$$

where

$$\mathbf{Q} = \begin{bmatrix} \mathcal{Q}^{-1/2} & \mathbf{0} \\ \mathbf{0} & \mathcal{Q}^{1/2} \end{bmatrix}, \quad \mathbf{P} = \begin{bmatrix} \mathcal{P}^{1/2} & \mathbf{0} \\ \mathbf{0} & \mathcal{P}^{1/2} \end{bmatrix}, \quad (58)$$

$$\mathcal{Q} = \text{diag}[\mathbf{Q}, \mathbf{Q}], \quad \mathcal{P} = \text{diag}[\mathbf{P}, \mathbf{P}], \quad (59)$$

$$\mathbf{Q} = \text{diag}[e^{i\mathbf{Q}_s \cdot (0, s_y, s_z)}], \quad \mathbf{P} = \text{diag}[e^{i\gamma_p \cdot s_z}]. \quad (60)$$

In the nomenclature of Sec. II D, we have denoted fields incident from above and below the layer by partitioned vectors of plane wave coefficients \mathcal{F}_1^\pm and outgoing fields by partitioned vectors \mathcal{F}_D^\pm [Eq. (51)]. In this section, it is more convenient to write \mathcal{F}_1^- and \mathcal{F}_2^+ , respectively, for the incoming fields above and below the layer, where these fields are now referred to the phase origins at P_1 and P_2 . The outgoing fields \mathcal{F}_1^+ (above the layer) and \mathcal{F}_2^- (below the layer) are expressed in terms of the interaction of the incident fields with the basic layer:

$$\mathcal{F}_1^+ = \mathcal{R}_a \mathcal{F}_1^- + \mathcal{T}_b \mathcal{F}_2^+, \quad (61)$$

$$\mathcal{F}_2^- = \mathcal{T}_a \mathcal{F}_1^- + \mathcal{R}_b \mathcal{F}_2^+. \quad (62)$$

From Eq. (56) and its magnetic analog, the total transverse electric and magnetic fields can be written as the vectors

$$\mathcal{E}_j = \mathcal{X}^{-1/2} (\mathcal{F}_j^- + \mathcal{F}_j^+), \quad (63)$$

$$\mathcal{K}_j = \mathcal{X}^{1/2} (\mathcal{F}_j^- - \mathcal{F}_j^+), \quad (64)$$

where $\mathcal{X} = \text{diag}[\xi, \xi^{-1}]$ and $\xi = \text{diag}[\gamma_s/k]$.

The \mathfrak{R} matrix is then introduced through the definition [30]

$$\begin{bmatrix} \mathcal{E}_1 \\ \mathcal{E}_2 \end{bmatrix} = \mathcal{X}^{-1/2} \begin{bmatrix} \mathfrak{R}_{11} & \mathfrak{R}_{12} \\ \mathfrak{R}_{21} & \mathfrak{R}_{22} \end{bmatrix} \mathcal{X}^{-1/2} \begin{bmatrix} \mathcal{K}_1 \\ \mathcal{K}_2 \end{bmatrix}, \quad (65)$$

¹Unrelated to the matrix \mathbf{T} in Sec. II D.

and by substituting Eq. (64) into Eq. (65) and setting \mathcal{F}_1^- and \mathcal{F}_2^+ in turn to $\mathbf{0}$, we form expressions that lead to the partition elements of \mathfrak{R} :

$$\mathfrak{R}_{11} = (\mathcal{Y}_1 + \mathcal{X}_2 \mathcal{X}_1)(\mathcal{I} - \mathcal{X}_2 \mathcal{X}_1)^{-1}, \quad (66)$$

$$\mathfrak{R}_{12} = -2\mathcal{Z}_1 \mathcal{X}_2 (\mathcal{I} - \mathcal{X}_1 \mathcal{X}_2)^{-1}, \quad (67)$$

$$\mathfrak{R}_{21} = 2\mathcal{Z}_2 \mathcal{X}_1 (\mathcal{I} - \mathcal{X}_2 \mathcal{X}_1)^{-1}, \quad (68)$$

$$\mathfrak{R}_{22} = -(\mathcal{Y}_2 + \mathcal{X}_1 \mathcal{X}_2)(\mathcal{I} - \mathcal{X}_1 \mathcal{X}_2)^{-1}, \quad (69)$$

where $\mathcal{Z}_j = (\mathcal{I} - \mathcal{R}_j)^{-1}$, $\mathcal{Y}_j = (\mathcal{I} + \mathcal{R}_j)\mathcal{Z}_j$, $\mathcal{X}_j = \mathcal{T}_j \mathcal{Z}_j$.

Solving Eqs. (64) and (65), we derive the cross layer transformation

$$\mathbf{G}_2 = \mathbf{M} \mathbf{G}_1, \quad (70)$$

where

$$\mathbf{G}_j = \begin{bmatrix} \mathcal{I} - \mathfrak{R}_{11} & \mathcal{I} + \mathfrak{R}_{11} \\ \mathcal{I} & -\mathcal{I} \end{bmatrix} \mathbf{F}_j, \quad (71)$$

with

$$\mathbf{M} = \begin{bmatrix} \mathfrak{R}_{22} - \mathfrak{R}_{11} & \mathcal{I} \\ \mathcal{I} & \mathbf{0} \end{bmatrix} \begin{bmatrix} \mathfrak{R}_{12}^{-1} & \mathbf{0} \\ \mathbf{0} & \mathfrak{R}_{21} \end{bmatrix} \quad (72)$$

and

$$\mathbf{F}_j = \begin{bmatrix} \mathcal{F}_j^- \\ \mathcal{F}_j^+ \end{bmatrix}, \quad \mathbf{G}_j = \begin{bmatrix} \mathcal{G}_j^- \\ \mathcal{G}_j^+ \end{bmatrix}. \quad (73)$$

The Bloch condition for field quasiperiodicity in the direction \mathbf{e}_3 imposes the constraint

$$\mathcal{F}_2^\pm = \mu \mathcal{F}_1^\pm \quad \text{with} \quad \mu = \exp(-i\mathbf{k}_0 \cdot \hat{\mathbf{e}}_z) \quad (74)$$

(where \mathbf{k}_0 denotes the Bloch vector) and, in turn, this requires that $\mathbf{G}_2 = \mu \mathbf{G}_1$, resulting in the eigenvalue problem $\mathbf{M} \mathbf{G}_1 = \mu \mathbf{G}_1$.

In its present form, the cross layer transformation matrix \mathbf{M} is just a reformulation of the \mathbf{T} matrix treatment. It thus suffers from the same ill conditioning that causes catastrophic numerical errors with increasing matrix dimension. These manifest themselves particularly in the case of 3D problems, for which the plane wave orders are doubly dimensioned. Here, the problem is associated with the inversion of \mathfrak{R}_{21}^{-1} , which, in turn, is related to the inversion of the transmission scattering matrices \mathcal{T} which occur in the \mathbf{T} matrix method. These problems are due to the peripheral entries of \mathcal{R} and \mathcal{T} , associated with highly evanescent input and output orders, becoming small with increasing order. While neither \mathcal{R} nor \mathcal{T} are well conditioned, a diagonally dominant matrix such as $\mathcal{I} - \mathcal{R}$ is well conditioned with increasing order.

These problems may be alleviated in various ways, all of which eliminate the necessity to invert the ill-conditioned matrices \mathfrak{R}_{12} and \mathfrak{R}_{21} . One approach, also adopted by Galak [17], is to consider the eigenproblem for a matrix

$\mathbf{M}' = (\mathbf{I} + \zeta \mathbf{M})^{-1}$ (ζ constant), the eigenvalues of which are $(1 + \zeta \mu)^{-1}$, from which the values of μ may be inferred. Some elementary manipulation inverts \mathbf{M}' analytically,

$$\mathbf{M}' = \begin{bmatrix} \mathfrak{R}_{12} \mathcal{D} & -\mathfrak{R}_{12} \mathcal{D} \mathfrak{R}_{21} \\ -\zeta \mathcal{D} & \mathcal{D} \{ \mathfrak{R}_{12} + \zeta (\mathfrak{R}_{22} - \mathfrak{R}_{11}) \} \end{bmatrix}, \quad (75)$$

$$\mathcal{D} = \{ \mathfrak{R}_{12} - \zeta^2 \mathfrak{R}_{21} + \zeta (\mathfrak{R}_{22} - \mathfrak{R}_{11}) \}^{-1}, \quad (76)$$

thus removing any numerical instabilities. While the value of ζ is chosen to avoid singular behavior, the values $\zeta = \pm 1$ generally suffice.

An alternative treatment involves the consideration of the modified matrix $\mathbf{M}'' = (\zeta \mathbf{M} + \zeta^{-1} \mathbf{M}^{-1})^{-1}$, the eigenvalues of which are $(\zeta \mu + \zeta^{-1} \mu^{-1})^{-1}$. Again, ill conditioning is eliminated by analytic inversion to yield

$$\mathbf{M}'' = \begin{bmatrix} \zeta^{-1} \mathfrak{R}_{12} & \mathbf{0} \\ \mathbf{0} & \mathbf{I} \end{bmatrix} \begin{bmatrix} \mathfrak{A} & \mathfrak{B} \\ \mathfrak{B} & -\mathfrak{A} \end{bmatrix}^{-1} \begin{bmatrix} \mathbf{I} & \mathbf{0} \\ \mathbf{0} & \zeta \mathfrak{R}_{21} \end{bmatrix}, \quad (77)$$

where $\mathfrak{A} = \mathfrak{R}_{22} - \mathfrak{R}_{11}$ and $\mathfrak{B} = \zeta^{-1} \mathfrak{R}_{12} + \zeta \mathfrak{R}_{21}$. The inverse in the central factor of Eq. (77) may be calculated analytically as before, or numerically, as this form is already well conditioned.

Appropriate values of ζ may easily be chosen, particularly for lattices and layers which exhibit high symmetry. In the case of structures such as the woodpile, for which the underlying layer (comprising crossed grating layers) does not exhibit a simplifying up-down symmetry, we utilize the preceding general technique with $\zeta = 1$.

In the case of the calculation of the space-filling modes of an air-guided holey fiber, the lattice is a 2D hexagonal structure composed of individual 1D cylinder gratings, each of which is up-down symmetric. In this case, the lattice replication vector is $\mathbf{e}_3 = (0, s_y, s_z)$, where $s_2 = d/2$, $s_3 = \sqrt{3}d/2$. This, in turn, simplifies the form of the lateral shift matrix \mathcal{Q} and introduces a natural choice for ζ . Here, $\mathcal{Q} = \zeta^{1/2} \mathcal{Q}_0$, with $\zeta = \exp(i\beta_0 d)$ and with $\mathcal{Q}_0 = \text{diag}(-1)^j$. The imposed lattice symmetry and relations in Eqs. (57) and (58) lead to $\mathcal{T}_j = \zeta^{2j-3} \mathcal{P} \mathcal{Q}_0 \mathcal{T}_0 \mathcal{Q}_0 \mathcal{P}_0$, together with analogous identities for the reflection matrices.

These, together with Eqs. (66)–(69), reduce $\mathfrak{R}_{22} = -\mathfrak{R}_{11}$ and $\zeta^{-1} \mathfrak{R}_{12} = -\zeta \mathfrak{R}_{21}$, thereby block diagonalizing \mathbf{M}' , Eq. (77), and halving the dimension of the eigenvalue problem. The Bloch factors μ may thus be inferred from the eigenvalues $(\zeta \mu + \zeta^{-1} \mu^{-1})^{-1}$ of $\zeta^{-1} \mathfrak{R}_{12} \mathfrak{R}_{22}^{-1}$.

In addition to the eigenvalues, it is advantageous in some situations to also characterize a semi-infinite crystal by a reflection scattering matrix \mathbf{R}_∞ , which can be derived from the eigenvectors. In all cases, we generate an eigenvector \mathbf{G} for each eigenvalue and infer from these the corresponding eigenvectors $\mathbf{F} = [\mathcal{F}^- \mathcal{F}^+]^T$ of the original problem. As discussed in Ref. [19], the eigenvalues are paired into forward and backward propagating states. For evanescent states, which carry no energy, those with eigenvalue $|\mu| < 1$ are regarded as forward propagating, while those with $|\mu| > 1$ are regarded as backward propagating.

For states that carry energy, the treatment is more delicate, requiring a calculation of the downward flux:

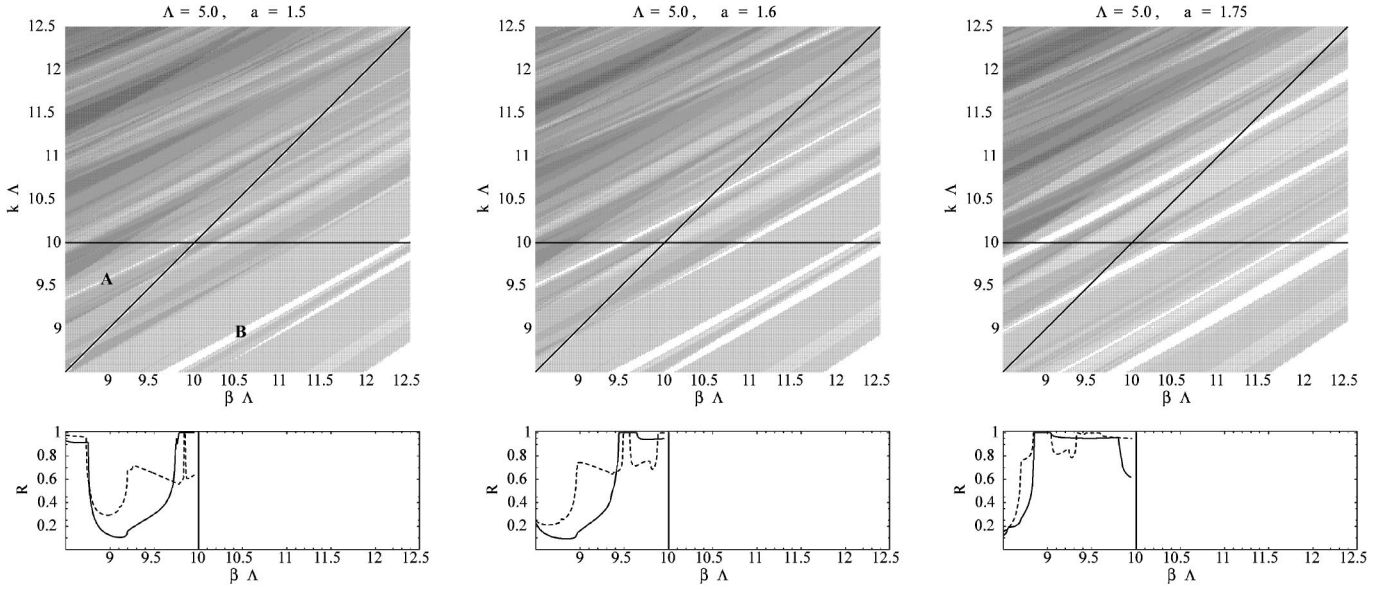


FIG. 4. Finger diagrams for a hexagonal array of air holes, in a silica matrix (refractive index $\nu=1.4897$), showing a plot of $k\Lambda$ versus $\beta\Lambda$ (both dimensionless) with $\Lambda=5.0\ \mu\text{m}$, using radii $a=1.5, 1.6,$ and $1.75\ \mu\text{m}$. The graphical representations below the finger diagrams depict reflectance of a semi-infinite crystal for various values of the Bloch vector and a fixed value $k\Lambda=10$. The dotted line represents the case where the component of the Bloch vector perpendicular to the grating plane lies on the path ΓKM on the border of the irreducible segment of the Brillouin zone. The solid line represents the case where the component of the Bloch vector perpendicular to the grating plane lies on the line ΓM .

$$E_F = \mathcal{F}_-^H \mathcal{I}_r \mathcal{F}_- - \mathcal{F}_+^H \mathcal{I}_r \mathcal{F}_+ - i \mathcal{F}_-^H \mathcal{I}_e \mathcal{F}_+ + i \mathcal{F}_+^H \mathcal{I}_e \mathcal{F}_- \quad n_{\text{eff}} = \beta/k, \quad (78) \quad (79)$$

[this equation may be derived from Eq. (C6)]. Those states with $E_F > 0$ are regarded as forward propagating, while those with $E_F < 0$ are backward propagating. With all modes partitioned as above, we form matrices $\hat{\mathbf{F}}_+$ and $\hat{\mathbf{F}}_-$, the columns of which are the vectors \mathcal{F}_+ and \mathcal{F}_- of the forward propagating states. Following Ref. [19], we form the reflection matrix $\mathbf{R}_\infty = \hat{\mathbf{F}}_+ \hat{\mathbf{F}}_-^{-1}$, from which we may compute the energy reflectance $\hat{\mathcal{R}}^H \mathcal{I}_r \hat{\mathcal{R}}$ from a corresponding incidence field \mathcal{D} , with $\hat{\mathcal{R}} = \mathbf{R}_\infty \mathcal{D}$.

IV. AIR-GUIDED MODES

We look now at the application of these tools to the guiding of light in air-cored optical fibers, the confinement mechanism of which is the photonic band gap. In these photonic crystal fibers, the light propagates in a large central hole in a silica matrix surrounded by a cladding, which consists of a hexagonal array of smaller air holes. For some modes, the bulk of the energy propagates in the central hole, allowing the possibility of low-loss propagation at those wavelengths for which the glass is highly absorbing.

The location of such modes is a delicate process and a demanding numerical task which we have commented briefly on previously [31], in the context of the multipole method [32,33], where what is required is to find a narrow minimum of a determinant as a function of a complex propagation constant. This quantity represents the variation of fields along the axis (Ox here) of the cylindrical holes, and is generally specified in terms of a complex effective index

where the fields vary axially as $\exp(i\beta x)$, and where k denotes the wave number in free space of the mode.² The real part of n_{eff} governs the propagation properties of the mode, while the imaginary part determines its energy loss during propagation through its lateral spread. This imaginary part has to be reduced to practically imposed values by increasing the number of rings of air holes [34].

The determination of air-guided modes requires two criteria to be simultaneously satisfied: first, the air holes surrounding the central hole must provide a “mirror” condition corresponding to the cladding array operated in a photonic band gap in which no propagating modes capable of carrying energy to infinity exist; second, the mode must satisfy an appropriate phase or propagation condition, i.e., an eigenvalue equation. Furthermore, for low-loss propagation we require the bulk of the light to propagate in air, necessitating that $n_{\text{eff}} \approx 1$, and a reasonable approximation to the propagation condition, namely, that the modes lie close to the light line [35], given by $\beta = k$.

The Bloch formulation of Sec. III provides us with a convenient method of specifying regions in the k - β plane in which the mirror condition of a total band gap is satisfied. The search for modes can then be carried out in localized regions of this plane, a feature we have found indispensable in our studies of air-guided modes.

We illustrate the effectiveness of this technique in Fig. 4,

²This use of β is at variance with that established in Sec. II B, but is standard optical fiber notation.

where we show that we call “finger diagrams,” named so for the fine unshaded (white) fingers that denote complete band gaps. These are plotted for a structure in which air holes of steadily increasing radius are used to confine a mode in a central hole of the type shown in Fig. 6. Each point on these diagrams shows the result of a search for modes as the Bloch vector traverses the edge of the irreducible segment of the Brillouin zone for an array of hexagonally packed air holes in a silica matrix, with a prescribed value of k and β . In fact [19] the side ΓM of the irreducible segment of the Brillouin zone is characterized by normal incidence on a grating with period $D = \Lambda$, the hexagonal array constant, and with $s_y = \Lambda/2$ and $s_z = \sqrt{3}\Lambda/2$, while the segment ΓKM is characterized by normal incidence on a grating with period $D = \sqrt{3}\Lambda$, and with $s_y = \sqrt{3}\Lambda/2$ and $s_z = \Lambda/2$. The finger diagrams are the result of scanning over a rectangular mesh in k - β space, searching for propagating states on the ΓM and ΓKM sides and shading the diagram according to the number of modes found—providing some indication of the “leakiness” of the confining structure. Unshaded (white) regions denote an absence of propagating modes and thus represent complete band gaps, the first requirement for air-guided modes. Our calculations are performed with a hybrid MATHEMATICA/FORTRAN code in which the scattering matrices are computed in a FORTRAN routine and communicated via MATHLINK to MATHEMATICA, in which the eigenvalue problem of Sec. III is solved and the finger diagram drawn. The method is quite efficient, requiring some 50 min of computation time for a 101×101 array in k - β space on a 600-MHz Pentium III system.

The graphs below the finger diagrams attempt to characterize the dispersion diagram for a fixed $k\Lambda = 10$ by displaying the reflectance of a semi-infinite array, illuminated at normal incidence from above corresponding to the Brillouin zone segments ΓM and ΓKM . This reflectance is calculated from the scattering matrix \mathbf{R}_∞ described in Sec. III. The dotted line is the case for which the component of the Bloch vector perpendicular to the grating plane lies on the path ΓKM [22] on the border of the irreducible segment of the Brillouin zone. For a given value of $\beta\Lambda$ and $k\Lambda$, this completely determines the Bloch vector. The solid line is the case where the component of the Bloch vector perpendicular to the grating plane lies on the segment ΓM .

Figure 4 displays finger diagrams³ for arrays of varying cylinder radius and it is evident that the confinement region of the finger labeled **A** widens with increasing air hole radius, and vanishes completely for normalized radius $a/\Lambda \leq 0.3$. That is, for holes with normalized radii less than 0.3, such air-guided modes can no longer be supported. Also note that not all confinement regions grow with air hole radius, as shown by the narrowing of the finger labeled **B** in Fig. 4. In Table I we give indicative figures for the widths of two prominent fingers in Fig. 4.

In all cases of Fig. 4, the width of finger **A** is determined by the ΓKM aspect, as exemplified in the lower graphs,

TABLE I. The width of a finger as a function of inclusions radius a and area fraction f , for a hexagonal array of air holes, in a silica matrix (refractive index $\nu = 1.4897$). The array constant is $\Lambda = 5.0 \mu\text{m}$.

a (μm)	f	Finger A	Finger B
1.75	0.444381	0.0616	0.0243
1.70	0.419350	0.0528	0.0657
1.65	0.395046	0.0449	0.0822
1.60	0.371466	0.0269	0.0818
1.55	0.348612	0.0090	0.0748
1.50	0.326484	0.0040	0.0736
1.45	0.305081	0.0000	0.0655

which show the total band gap with a 100% reflectance. Total band gaps, however, are not a necessary condition for the air-guided modes, as exemplified in Fig. 2 of White *et al.* [31], in which modes have been found outside the total confinement finger, but which lie within the ΓM aspect.

Figure 5, shows the finger diagram, the dispersion curve for an air-guided mode, and the light line for a photonic crystal fiber with specified geometry. The location of the dispersion curve on the high-frequency side of the light line implies that the guiding mechanism cannot be total internal reflection, but instead must arise through band-gap effects. We do not detail the method by which these are located but refer the reader to our multipole treatment [31–33]. The mode of Fig. 6 was found by searching in finger **A** of Fig. 4.

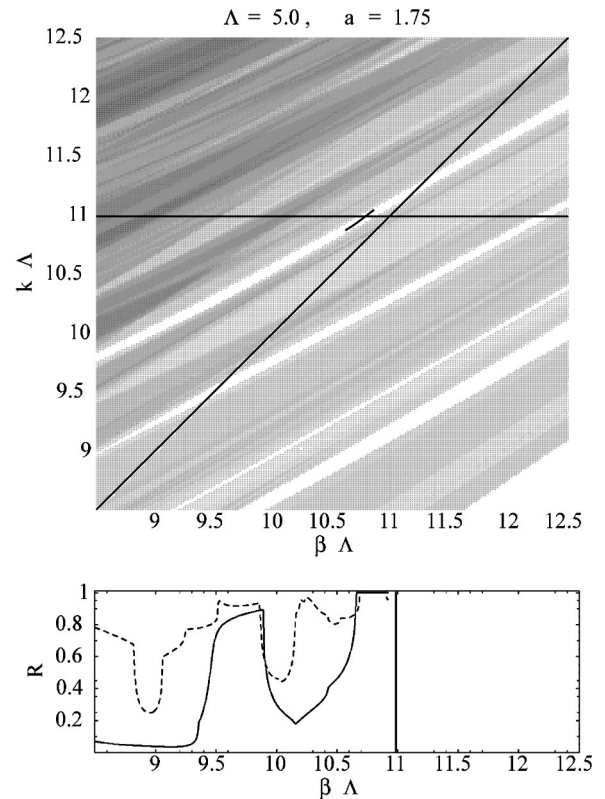


FIG. 5. Dispersion curve for the mode shown in Fig. 6, with $\Lambda = 5.0 \mu\text{m}$ and $a = 1.75 \mu\text{m}$.

³A full color version of Fig. 6 may be viewed at our website <http://www.physics.usyd.edu.au/theory/dif/node7.html>

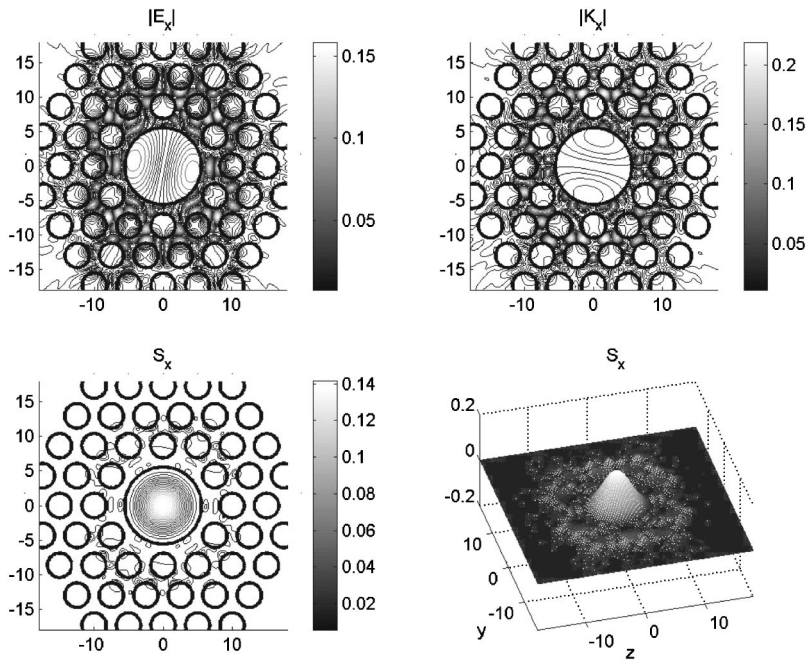


FIG. 6. A mode confined in a central air hole, of radius $5.55 \mu\text{m}$, in a silica matrix, by a set of three layers of air holes hexagonally packed. The hexagonal structure around the central hole consists of a finite set of air holes (radius $a = 1.75 \mu\text{m}$), in a silica matrix (refractive index $\nu = 1.4897$), and corresponds to a hexagonal array of constant $\Lambda = 5.0 \mu\text{m}$. The top two contour plots display electric and scaled magnetic field magnitudes, while the lower two graphs display the axial Poynting vector.

V. CONCLUSION

The theory described in this paper, for the conical diffraction of plane waves by dielectric or metallic cylinder gratings, is an important addition to our tool kit of computational methods for photonic crystal structures. The method generates plane wave reflection and transmission scattering matrices, which are the basic building blocks of energy and propagation property calculations. In this paper, the theory is formulated in a general fashion, enabling its use in the construction of 2D stacks of 1D gratings, and its future use in the study of the 3D stacks in the woodpile configuration. We have also outlined a computationally robust formulation of the Bloch problem for propagation characteristics of 2D and 3D arrays, and have described elegant simplifications that halve the dimension of the eigenproblem for highly symmetric structures. These tools have underpinned our numerical studies of guided modes in air-cored photonic crystal fibers [31] and have proved to be both efficient and accurate. We have exemplified the use of the method and numerically demonstrated relationships between the width of total band-gap fingers in the dispersion diagram and the radius of the holes in the cladding.

The generalization of the methods described here to gratings having cylinders composed of metallic or lossy materials is immediate, and no numerical problems arise, with the sole change being that the boundary condition elements defined in Appendix A involve complex quantities. As with all multipole methods, the field representation in Wijnngaard multipole expansions is quite efficient, yielding good computational accuracy for relatively small computational times. While the detail of theory that is described here refers only to circular cylinders, the general framework is amenable to noncircular cylinders, requiring only the replacement of the “impedance” matrices \mathcal{M} in the modal scattering operator $(\mathcal{M} + \mathcal{S})^{-1}$. This separation of the lattice geometry encapsulated in lattice sums which populate \mathcal{S} and the material

properties of the structure which are contained within \mathcal{M} is a computationally attractive feature that is common to all Rayleigh multipole methods. The introduction of conical diffraction is most significantly reflected in the lattice sums which now involve a projected wave number k_{\perp} in accordance with Maystre’s theorem. When the axial component of the wave vector is sufficiently large, k_{\perp} becomes imaginary. In the context of the examples in his paper, this occurs when the light line is crossed. The issue is of greatest significance, however, in the case of a cross grating such as the woodpile in which the diffracted plane wave set is doubly dimensioned and imaginary values of k_{\perp} arise routinely. Fortunately, this causes little problem as the lattice sum series converges very rapidly. Indeed, our computational methods [18] based on the work of Ref. [36] readily extend to accommodate this case. As a final aside, we note that the theory of conical diffraction, when operated in-plane, generates in a block diagonal structure the scattering matrices for both principal polarizations.

Finally, we note that the paper outlines a number of general conservation relations for lossless structures, derived from energy conservation, applicable to 2D and 3D structures. For multipole formulations, these are analytically conserved, independently of series truncation, while for other techniques they provide convergence tests. In our context, we have found these identities to be an invaluable aid in the testing of our code.

ACKNOWLEDGMENTS

The authors acknowledge financial support from the Australian Research Council, and helpful discussions with C. M. de Sterke and T. P. White.

APPENDIX A: BOUNDARY CONDITIONS

The field in the vicinity of each cylinder is expressed in terms of cylindrical harmonics. Thus, in the vicinity of the central cylinder we write

$$E_x(r, \theta) = \sum_{n=-\infty}^{\infty} [A_n^{(E)} J_n(k_{\perp} r) + B_n^{(E)} H_n^{(1)}(k_{\perp} r)] e^{in\theta} e^{ik_{\parallel} x}, \quad (\text{A1})$$

$$K_x(r, \theta) = \sum_{n=-\infty}^{\infty} [A_n^{(K)} J_n(k_{\perp} r) + B_n^{(K)} H_n^{(1)}(k_{\perp} r)] e^{in\theta} e^{ik_{\parallel} x}, \quad (\text{A2})$$

with $e^{ik_{\parallel} x}$ denoting the x dependence of the fields. These series converge in an annular region bounded inwardly by $r=a$ and outwardly by the radial distance to the next field source located at the center of the nearest adjacent cylinder. Within each cylinder of radius a , the field is given by the regular expansion

$$E_x(r, \theta) = \sum_{n=-\infty}^{\infty} C_n^{(E)} J_n(\nu k_{\perp} r) e^{in\theta} e^{ik_{\parallel} x}, \quad (\text{A3})$$

$$K_x(r, \theta) = \sum_{n=-\infty}^{\infty} C_n^{(K)} J_n(\nu k_{\perp} r) e^{in\theta} e^{ik_{\parallel} x}, \quad (\text{A4})$$

where ν denotes the refractive index of the cylinders. At the cylinder boundaries E_x , K_x , E_{θ} and K_{θ} are continuous. We can find E_x and K_x from Eqs. (A1)–(A4), while the following equations [37]:

$$\mathbf{E}_{yz} = \frac{i}{k_{\perp}^2} (k_{\parallel} \nabla_{yz} E_x - k \hat{\mathbf{x}} \times \nabla_{yz} K_x), \quad (\text{A5})$$

$$\mathbf{K}_{yz} = \frac{i}{k_{\perp}^2} (k \epsilon_r \hat{\mathbf{x}} \times \nabla_{yz} E_x + k_{\parallel} \nabla_{yz} K_x), \quad (\text{A6})$$

which follow from Maxwell's equations, together with the relations $E_{\theta} = \mathbf{E}_{yz} \cdot \hat{\boldsymbol{\theta}}$ and $K_{\theta} = \mathbf{K}_{yz} \cdot \hat{\boldsymbol{\theta}}$, can be used to find expressions for E_{θ} and K_{θ} .

We find, after some simplification, that the boundary conditions imply

$$A_n^{(E)} J_n(k_{\perp}^e a) + B_n^{(E)} H_n(k_{\perp}^e a) = C_n^{(E)} J_n(k_{\perp}^i a), \quad (\text{A7})$$

$$A_n^{(K)} J_n(k_{\perp}^e a) + B_n^{(K)} H_n(k_{\perp}^e a) = C_n^{(K)} J_n(k_{\perp}^i a), \quad (\text{A8})$$

$$\begin{aligned} A_n^{(E)} J_n'(k_{\perp}^e a) + B_n^{(E)} H_n^{(1)'}(k_{\perp}^e a) \\ = c_1 C_n^{(E)} J_n'(k_{\perp}^i a) + c_2 n C_n^{(K)} J_n(k_{\perp}^i a), \end{aligned} \quad (\text{A9})$$

$$\begin{aligned} A_n^{(K)} J_n'(k_{\perp}^e a) + B_n^{(K)} H_n^{(1)'}(k_{\perp}^e a) \\ = -c_2 n C_n^{(E)} J_n(k_{\perp}^i a) + c_3 C_n^{(K)} J_n'(k_{\perp}^i a). \end{aligned} \quad (\text{A10})$$

In these equations, the constants c_1 , c_2 , and c_3 are defined by

$$c_1 = \frac{k_{\perp}^e \epsilon_r}{k_{\perp}^i}, \quad c_2 = \frac{ik_{\parallel}}{ak_{\perp}^e k_0} \left[\left(\frac{k_{\perp}^e}{k_{\perp}^i} \right)^2 - 1 \right], \quad c_3 = \frac{k_{\perp}^e}{k_{\perp}^i}, \quad (\text{A11})$$

where $k_{\perp}^e = k_{\perp}$ and $k_{\perp}^i = \sqrt{\nu^2 k^2 - k_{\parallel}^2}$.

We can now eliminate $\{C_n^{(E)}\}$ and $\{C_n^{(K)}\}$ from Eqs. (A7)–(A10). In order to express the result of this calculation in a compact form, we introduce the nomenclature

$$\mathcal{J}(c) = \frac{J_n'(k_{\perp}^e a)}{J_n(k_{\perp}^e a)} - c \frac{J_n'(k_{\perp}^i a)}{J_n(k_{\perp}^i a)}, \quad (\text{A12})$$

$$\mathcal{H}(c) = \frac{H_n'(k_{\perp}^e a)}{H_n(k_{\perp}^e a)} - c \frac{J_n'(k_{\perp}^i a)}{J_n(k_{\perp}^i a)}. \quad (\text{A13})$$

The result can be expressed in the form

$$\begin{bmatrix} A_n^{(E)} \\ A_n^{(K)} \end{bmatrix} = - \begin{bmatrix} M_n^{EE} & M_n^{EK} \\ M_n^{KE} & M_n^{KK} \end{bmatrix} \begin{bmatrix} B_n^{(E)} \\ B_n^{(K)} \end{bmatrix}, \quad (\text{A14})$$

where

$$M_n^{EE} = \frac{1}{\Delta_n} \frac{H_n(k_{\perp}^e a)}{J_n(k_{\perp}^e a)} [c_2^2 n^2 + \mathcal{J}(c_3) \mathcal{H}(c_1)], \quad (\text{A15})$$

$$M_n^{EK} = -M_n^{KE} = \frac{1}{\Delta_n} \left[\frac{1}{J_n(k_{\perp}^e a)} \right]^2 \frac{2ic_2}{\pi k_{\perp}^e a} n, \quad (\text{A16})$$

$$M_n^{KK} = \frac{1}{\Delta_n} \frac{H_n(k_{\perp}^e a)}{J_n(k_{\perp}^e a)} [c_2^2 n^2 + \mathcal{J}(c_1) \mathcal{H}(c_3)], \quad (\text{A17})$$

and

$$\Delta_n = \mathcal{J}(c_1) \mathcal{J}(c_3) + c_2^2 n^2. \quad (\text{A18})$$

It is easy to see that M_n^{EK} and M_n^{KE} are real. Furthermore, a little straightforward manipulation shows that

$$\begin{aligned} M_n^{EE} &= 1 + i\lambda_1, \\ M_n^{KK} &= 1 + i\lambda_2, \end{aligned} \quad (\text{A19})$$

where λ_1 and λ_2 are real.

In the case where $\mathbf{k}_i = (0, \beta_0, -\gamma_0)$, that is, $\phi = \pi/2$, Eqs. (A15)–(A17) simplify to those given in Ref. [18]:

$$M_n^{EE} = \frac{\nu J_n'(vka) H_n(ka) - J_n(vka) H_n'(ka)}{\nu J_n'(vka) J_n(ka) - J_n(vka) J_n'(ka)}, \quad (\text{A20})$$

$$M_n^{EK} = M_n^{KE} = 0, \quad (\text{A21})$$

$$M_n^{KK} = \frac{J_n'(vka) H_n(ka) - \nu J_n(vka) H_n'(ka)}{J_n'(vka) J_n(ka) - \nu J_n(vka) J_n'(ka)}. \quad (\text{A22})$$

APPENDIX B: SYMMETRY OPERATIONS AND FOLDING

In this section we show how up-down symmetry reduces the computational complexity of the formulation. In the first instance, we show that the blocks $\mathcal{K}^s \mathcal{L} \mathcal{J}^a$ and $\mathcal{K}^a \mathcal{L} \mathcal{J}^s$ vanish in the case of up-down symmetry. Next, we derive a folding procedure, which halves the number of equations.

Through the use of the matrix \mathbf{C} to decompose the fields into symmetric and antisymmetric components, the Rayleigh identity (27) may be written as

$$\mathfrak{B} = -\frac{1}{2}(\mathcal{M} + \mathcal{S})^{-1}[\mathcal{J}^s \mathcal{J}^a] \mathbf{C} \mathbf{D}. \quad (\text{B1})$$

We may get two equations from Eq. (B1), one involving \mathcal{J}^s and the other involving \mathcal{J}^a . For the \mathcal{J}^s case, let us suppose that $[(\mathbf{B}^E)^T (\mathbf{B}^K)^T]^T$ is a solution of the equation

$$(\mathcal{M} + \mathcal{S}) \begin{bmatrix} \mathbf{B}^E \\ \mathbf{B}^K \end{bmatrix} = \mathcal{J}^s \begin{bmatrix} \mathbf{X}_1 \\ \mathbf{X}_2 \end{bmatrix}, \quad (\text{B2})$$

with $[\mathbf{X}_1^T \mathbf{X}_2^T]^T = (\mathbf{C} \mathbf{D})_1$. Then

$$\begin{bmatrix} \mathbf{M}^{EE} \mathbf{B}^E + \mathbf{S} \mathbf{B}^E + \mathbf{M}^{EK} \mathbf{B}^K \\ \mathbf{M}^{KE} \mathbf{B}^E + \mathbf{S} \mathbf{B}^K + \mathbf{M}^{KK} \mathbf{B}^K \end{bmatrix} = \begin{bmatrix} \mathbf{J}^\oplus \mathbf{X}_1 \\ \mathbf{J}^\ominus \mathbf{X}_2 \end{bmatrix}. \quad (\text{B3})$$

Let $\mathbf{U} = \text{diag}[(-1)^m]$ and let the reversing matrix \mathbf{P} be the matrix with secondary diagonal terms equal to unity and all other terms equal to zero, that is, $\mathbf{P} = [\delta_{-m,n}]$. The symmetries $M_n^{EE} = M_{-n}^{EE}$, $M_n^{KK} = M_{-n}^{KK}$, $M_n^{KE} = -M_{-n}^{KE}$, and $M_n^{EK} = -M_{-n}^{EK}$, which follow from Eqs. (A15)–(A17), and are a consequence of the up-down symmetry for a uniform cylinder grating, allow us to deduce that

$$\mathbf{P} \mathbf{U} \mathbf{M}^{EE} \mathbf{U} \mathbf{P} = \mathbf{M}^{EE}, \quad \mathbf{P} \mathbf{U} \mathbf{M}^{KK} \mathbf{U} \mathbf{P} = \mathbf{M}^{KK},$$

$$\mathbf{P} \mathbf{U} \mathbf{M}^{EK} \mathbf{U} \mathbf{P} = -\mathbf{M}^{EK}, \quad \mathbf{P} \mathbf{U} \mathbf{M}^{KE} \mathbf{U} \mathbf{P} = -\mathbf{M}^{KE}, \quad (\text{B4})$$

while from $S_m = (-1)^m S_{-m}$ we deduce

$$\mathbf{P} \mathbf{U} \mathbf{S} \mathbf{U} \mathbf{P} = \mathbf{S}. \quad (\text{B5})$$

Substitution of these results into Eq. (B3) and resultant simplification leads to

$$(\mathcal{M} + \mathcal{S}) \begin{bmatrix} \mathbf{P} \mathbf{U} \mathbf{B}^E \\ -\mathbf{P} \mathbf{U} \mathbf{B}^K \end{bmatrix} = \mathcal{J}^s \begin{bmatrix} \mathbf{X}_1 \\ \mathbf{X}_2 \end{bmatrix}, \quad (\text{B6})$$

showing that

$$\mathbf{B}^E = \mathbf{P} \mathbf{U} \mathbf{B}^E, \quad \mathbf{B}^K = -\mathbf{P} \mathbf{U} \mathbf{B}^K, \quad (\text{B7})$$

since Eq. (B2) has a unique solution.

We now have

$$\mathcal{K}^a (\mathcal{M} + \mathcal{S})^{-1} \mathcal{J}^s = \mathcal{K}^a \begin{bmatrix} \mathbf{B}^E \\ \mathbf{B}^K \end{bmatrix} = \begin{bmatrix} \mathbf{K}^\ominus \mathbf{B}^E \\ \mathbf{K}^\oplus \mathbf{B}^K \end{bmatrix}. \quad (\text{B8})$$

Using Eqs. (B7) and the results $\mathbf{K}^\ominus = -\mathbf{K}^\ominus \mathbf{U} \mathbf{P}$, $\mathbf{K}^\oplus = \mathbf{K}^\oplus \mathbf{U} \mathbf{P}$, we deduce that $\mathbf{K}^\ominus \mathbf{B}^E = 0$ and $\mathbf{K}^\oplus \mathbf{B}^K = 0$. Thus

$$\mathcal{K}^a (\mathcal{M} + \mathcal{S})^{-1} \mathcal{J}^s = 0. \quad (\text{B9})$$

Similarly

$$\mathcal{K}^s (\mathcal{M} + \mathcal{S})^{-1} \mathcal{J}^a = 0. \quad (\text{B10})$$

These considerations show that the system (37) decouples completely for gratings having an up-down symmetry.

Finally, we note that we can reduce computational complexity by ‘‘folding’’ the equations, thus reducing their number by a factor of 2. Consider the expression $\mathcal{K}^s \mathcal{L} \mathcal{J}^s (\mathbf{C} \mathbf{D})_1$ appearing in Eq. (37). The above methods show that if

$$[\mathbf{B}^E \ \mathbf{B}^K]^T = \mathcal{L} \mathcal{J}^s (\mathbf{C} \mathbf{D})_1, \quad (\text{B11})$$

then $[\mathbf{B}^E \ \mathbf{B}^K]^T = [\mathbf{P} \mathbf{U} \mathbf{B}^E \ -\mathbf{P} \mathbf{U} \mathbf{B}^K]^T$. Consequently, after some matrix manipulation, we have

$$\mathcal{K}^s \begin{bmatrix} \mathbf{B}^E \\ \mathbf{B}^K \end{bmatrix} = 2 \begin{bmatrix} \tilde{\mathbf{K}}^\oplus \tilde{\mathbf{B}}^E \\ \tilde{\mathbf{K}}^\ominus \tilde{\mathbf{B}}^K \end{bmatrix} \stackrel{\text{def}}{=} 2 \tilde{\mathcal{K}}^s \begin{bmatrix} \tilde{\mathbf{B}}^E \\ \tilde{\mathbf{B}}^K \end{bmatrix}, \quad (\text{B12})$$

where the tilde denotes a folded matrix, that is, $\tilde{\mathbf{K}}^{\oplus/\ominus} = [\mathbf{K}_{sn}^{\oplus/\ominus}]$, $n \geq 0$ and $\tilde{\mathbf{B}}^{E/K} = [\mathbf{B}_n^{E/K}]$, $n \geq 0$.

After a straightforward calculation, we find from Eq. (B11) that

$$\begin{bmatrix} \tilde{\mathbf{B}}^E \\ \tilde{\mathbf{B}}^K \end{bmatrix} = \begin{bmatrix} \tilde{\mathcal{M}}^{EE} \epsilon^{-1} + \tilde{\sigma}^\oplus & \tilde{\mathcal{M}}^{EK} \\ \tilde{\mathcal{M}}^{KE} & \tilde{\mathcal{M}}^{KK} \epsilon^{-1} + \tilde{\sigma}^\ominus \end{bmatrix}^{-1} \tilde{\mathcal{J}}^s (\mathbf{C} \mathbf{D})_1, \quad (\text{B13})$$

where $[\tilde{\sigma}_{mn}^{\oplus/\ominus}] = [\mathbf{S}_{m-n} + (-1)^n \mathbf{S}_{m+n}]$, $m, n \geq 0$ and

$$\epsilon = \text{diag}[\epsilon_m], \quad \epsilon_m = \begin{cases} 1/2 & \text{if } m = 0 \\ 1 & \text{if } m > 0, \end{cases} \quad (\text{B14})$$

denotes the Neumann symbol.

Thus $\mathcal{K}^s \mathcal{L} \mathcal{J}^s (\mathbf{C} \mathbf{D})_1 = 2 \tilde{\mathcal{K}}^s \tilde{\mathcal{L}} \tilde{\mathcal{J}}^s (\mathbf{C} \mathbf{D})_1$ and similarly $\mathcal{K}^a \mathcal{L} \mathcal{J}^a (\mathbf{C} \mathbf{D})_2 = 2 \tilde{\mathcal{K}}^a \tilde{\mathcal{L}} \tilde{\mathcal{J}}^a (\mathbf{C} \mathbf{D})_2$. Hence, for up-down symmetric gratings we can write Eq. (48) as

$$\mathbf{S} = \mathbf{I} - \frac{2k}{k_\perp^2 D} \mathbf{X} \begin{bmatrix} \tilde{\mathcal{K}}^s \tilde{\mathcal{L}} \tilde{\mathcal{J}}^s & \mathbf{0} \\ \mathbf{0} & \tilde{\mathcal{K}}^a \tilde{\mathcal{L}} \tilde{\mathcal{J}}^a \end{bmatrix} \mathbf{X}. \quad (\text{B15})$$

The matrices

$$\begin{aligned} \mathbf{S}^\oplus &= \mathbf{I} - \frac{2k}{k_\perp^2 D} \mathcal{X} \tilde{\mathcal{K}}^s \tilde{\mathcal{L}} \tilde{\mathcal{J}}^s \mathcal{X}, \\ \mathbf{S}^\ominus &= \mathbf{I} - \frac{2k}{k_\perp^2 D} \mathcal{X} \tilde{\mathcal{K}}^a \tilde{\mathcal{L}} \tilde{\mathcal{J}}^a \mathcal{X} \end{aligned} \quad (\text{B16})$$

are the scattering matrices corresponding to the symmetric and antisymmetric problems discussed in Ref. [18].

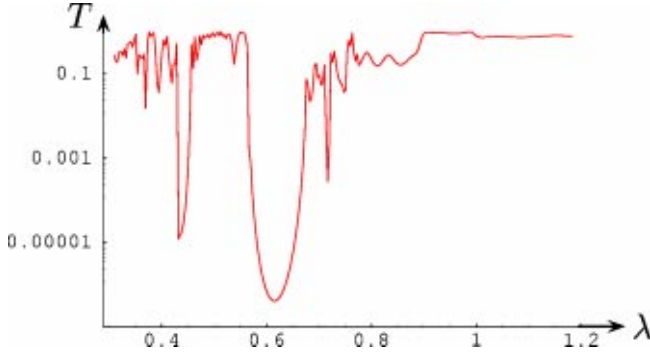


FIG. 7. Graph showing the transmittance T for ten parallel layers of cylinders as a function of wavelength λ for TM polarization. The incidence parameters are $\alpha_0=0.3$, $\beta_0=0.5$, and $\gamma_0=1$ (μm) $^{-1}$. The cylinder radii are $0.09 \mu\text{m}$, the layer periodicity is $0.25 \mu\text{m}$, and the layer separation (center to center) is $0.22 \mu\text{m}$.

APPENDIX C: VERIFICATION OF THE CODE

1. Convergence tests

Figure 7 shows the transmittance for TM polarization as a function of wavelength for a ten-layer stack of cylinder gratings in a square array. The incidence parameters are $\alpha_0=0.3$, $\beta_0=0.5$, and $\gamma_0=1$. The cylinder radii are $0.09 \mu\text{m}$, the layer periodicity is $0.25 \mu\text{m}$, and the layer separation (center to center) is $0.22 \mu\text{m}$. We let the number of cylindrical harmonics such as in Eqs. (17) and (18) be $2N_h+1$ and we let the number of plane wave orders in representations such as Eq. (28) be $2N_p+1$. Tables II and III show that stability is achieved for only a modest number of terms.

2. Energy conservation

From

$$\nabla \cdot (\mathbf{E} \times \mathbf{H}^*) = i\omega(\mu_0 |\mathbf{H}|^2 - \epsilon^* |\mathbf{E}|^2), \quad (\text{C1})$$

which follows from Maxwell's equations, and an application of Gauss's theorem to $\mathbf{E} \times \mathbf{H}^* - \mathbf{E}^* \times \mathbf{H}$ over the region $A = U \setminus C$ between the cross section C of a cylinder and the unit cell U (Fig. 2), it follows that for lossless cylinders

$$\text{Re} \left\{ \int_{U^+} \hat{\mathbf{z}} \cdot \mathbf{E} \times \mathbf{H}^* ds \right\} = \text{Re} \left\{ \int_{U^-} \hat{\mathbf{z}} \cdot \mathbf{E} \times \mathbf{H}^* ds \right\}, \quad (\text{C2})$$

that is,

TABLE II. Table showing convergence of the transmittance for ten parallel layers of cylinders at a wavelength $\lambda=0.385 \mu\text{m}$. The parameters N_h and N_p , as well as the physical specifications of the system are described in the text and in the caption of Fig. 7.

	$N_h=2$	$N_h=4$	$N_h=6$	$N_h=8$	$N_h=10$	$N_h=12$
$N_p=2$	0.943521	0.916007	0.915795	0.915789	0.915789	0.915789
$N_p=3$	0.943530	0.915960	0.915739	0.915731	0.915730	0.915730
$N_p=4$				0.915730	0.915729	0.915729
$N_p=5$					0.915729	0.915729
$N_p=6$					0.915729	0.915729

$$\text{Re} \left\{ \int_{U^+} \mathbf{E}_t \cdot \hat{\mathbf{z}} \times \mathbf{K}_t^* ds \right\} = \text{Re} \left\{ \int_{U^-} \mathbf{E}_t \cdot \hat{\mathbf{z}} \times \mathbf{K}_t^* ds \right\}. \quad (\text{C3})$$

We now substitute Eqs. (6) and (7) into Eq. (C3). After simplification, we find that the downward fluxes at U^+ and U^- are related by

$$\begin{aligned} & \sum_{s \in \Omega_r} [(|E_{I,s}^-|^2 + |F_{I,s}^-|^2) - (|E_{D,s}^+|^2 + |F_{D,s}^+|^2)] \\ & - i \sum_{s \in \Omega_e} [(E_{I,s}^- * E_{D,s}^+ - F_{I,s}^- * F_{D,s}^+) \\ & - (E_{I,s}^+ * E_{D,s}^- - F_{I,s}^+ * F_{D,s}^-)] \\ & = \sum_{s \in \Omega_r} [(|E_{D,s}^-|^2 + |F_{D,s}^-|^2) - (|E_{I,s}^+|^2 + |F_{I,s}^+|^2)] \\ & - i \sum_{s \in \Omega_e} [(E_{D,s}^- * E_{I,s}^+ - F_{D,s}^- * F_{I,s}^+) \\ & - (E_{D,s}^+ * E_{I,s}^- - F_{D,s}^+ * F_{I,s}^-)], \end{aligned} \quad (\text{C4})$$

where the sets Ω_r and Ω_e have been defined in Eqs. (3) and (4).

The various terms of Eq. (C4) can be written in matrix form. For example,

$$\sum_{s \in \Omega_r} |E_{D,s}^+|^2 = (\mathbf{E}_D^+)^H \mathbf{I}_r \mathbf{E}_D^+,$$

$$\sum_{s \in \Omega_e} E_{I,s}^- * E_{D,s}^+ = (\mathbf{E}_I^-)^H \mathbf{I}_e \mathbf{E}_D^+. \quad (\text{C5})$$

Here, \mathbf{I}_r and \mathbf{I}_e are unit diagonal projection matrices that, respectively, select the (real) propagating and the evanescent orders. That is, $[\mathbf{I}_r]_{pq} = \delta_{pq}$ for $p \in \Omega_r$ and 0 otherwise. Correspondingly, $[\mathbf{I}_e]_{pq} = \delta_{pq}$ for $p \in \Omega_e$ and 0 otherwise, and thus $\mathbf{I}_r + \mathbf{I}_e = \mathbf{I}$ and $\mathbf{I}_r \mathbf{I}_e = \mathbf{0}$.

In turn, using the composite nomenclature of Eq. (51), the energy fluxes at U^+ and U^- reduce to

TABLE III. As for Table II, but at a wavelength $\lambda = 0.61 \mu\text{m}$.

	$N_h=2$	$N_h=4$	$N_h=6$	$N_h=8$	$N_h=10$	$N_h=12$
$N_p=2$	6.111972×10^{-7}	4.390910×10^{-7}	4.381656×10^{-7}	4.381086×10^{-7}	4.381076×10^{-7}	4.381076×10^{-7}
$N_p=3$	6.117160×10^{-7}	4.393621×10^{-7}	4.384274×10^{-7}	4.383649×10^{-7}	4.383633×10^{-7}	4.383633×10^{-7}
$N_p=4$				4.383666×10^{-7}	4.383650×10^{-7}	4.383649×10^{-7}
$N_p=5$					4.383650×10^{-7}	4.383649×10^{-7}
$N_p=6$					4.383650×10^{-7}	4.383649×10^{-7}

$$\mathcal{F}_I^{-H} \mathcal{I}_r \mathcal{F}_I^- - \mathcal{F}_D^{+H} \mathcal{I}_r \mathcal{F}_D^+ - i \mathcal{F}_I^{-H} \mathcal{I}_e \mathcal{F}_D^+ \quad \mathbf{S}^H \mathbf{I}_r \mathbf{S} = \mathbf{I}_r - i \mathbf{I}_e \mathbf{S} + i \mathbf{S}^H \mathbf{I}_e. \quad (\text{C11})$$

$$+ i \mathcal{F}_D^{+H} \mathcal{I}_e \mathcal{F}_I^- = \mathcal{F}_D^{-H} \mathcal{I}_r \mathcal{F}_D^- - \mathcal{F}_I^{+H} \mathcal{I}_r \mathcal{F}_I^+ \\ - i \mathcal{F}_D^{-H} \mathcal{I}_e \mathcal{F}_I^+ + i \mathcal{F}_I^{+H} \mathbf{I}_e \mathcal{F}_D^-, \quad (\text{C6})$$

where $\mathcal{I}_r = \text{diag}[\mathbf{I}_r, \mathbf{I}_r]$ and $\mathcal{I}_e = \text{diag}[\mathbf{I}_e, -\mathbf{I}_e]$.

By substituting the following relationships (expressed in terms of scattering matrices) between the outgoing and incident fields:

$$\mathcal{F}_D^+ = \mathcal{R}_a \mathcal{F}_I^- + \mathcal{T}_b \mathcal{F}_I^+ \quad (\text{C7})$$

$$\mathcal{F}_D^- = \mathcal{T}_a \mathcal{F}_I^- + \mathcal{R}_b \mathcal{F}_I^+, \quad (\text{C8})$$

into Eq. (C6), we derive

$$\mathbf{F}_I^H [\mathbf{I}_r - \mathbf{S}^H \mathbf{I}_r \mathbf{S} - i \mathbf{I}_e \mathbf{S} + i \mathbf{S}^H \mathbf{I}_e] \mathbf{F}_I = \mathbf{0}, \quad (\text{C9})$$

where $\mathbf{F}_I = [(\mathcal{F}_I^-)^T (\mathcal{F}_I^+)^T]^T$ and

$$\mathbf{S} = \begin{bmatrix} \mathcal{R}_a & \mathcal{T}_b \\ \mathcal{T}_a & \mathcal{R}_b \end{bmatrix}, \quad \mathbf{I}_{r/e} = \begin{bmatrix} \mathcal{I}_{r/e} & \mathbf{0} \\ \mathbf{0} & \mathcal{I}_{r/e} \end{bmatrix}. \quad (\text{C10})$$

Since Eq. (C9) must hold for all \mathbf{F}_I , we conclude that

Extracting the four partitions, we derive

$$\mathcal{T}_a^H \mathcal{I}_r \mathcal{T}_a + \mathcal{R}_a^H \mathcal{I}_r \mathcal{R}_a = \mathcal{I}_r - i \mathcal{I}_e \mathcal{R}_a + i \mathcal{R}_a^H \mathcal{I}_e, \quad (\text{C12})$$

$$\mathcal{T}_a^H \mathcal{I}_r \mathcal{R}_b + \mathcal{R}_a^H \mathcal{I}_r \mathcal{T}_b = -i \mathcal{I}_e \mathcal{T}_b + i \mathcal{T}_a^H \mathcal{I}_e, \quad (\text{C13})$$

$$\mathcal{R}_b^H \mathcal{I}_r \mathcal{T}_a + \mathcal{T}_b^H \mathcal{I}_r \mathcal{R}_a = -i \mathbf{I}_e \mathcal{T}_a + i \mathcal{T}_b^H \mathcal{I}_e, \quad (\text{C14})$$

$$\mathcal{R}_b^H \mathcal{I}_r \mathcal{R}_b + \mathcal{T}_b^H \mathcal{I}_r \mathcal{T}_b = \mathcal{I}_r - i \mathcal{I}_e \mathcal{R}_b + i \mathcal{R}_b^H \mathcal{I}_e. \quad (\text{C15})$$

The energy conservation relationships (C11)–(C15) rely entirely on physical principles. However, a generalization of the argument in Sec. 3 A 2 of Ref. [21] shows that these conservation properties are embedded in the modal formulation and preserved to within machine precision in any computational implementation. In a computational sense, while Eqs. (C11)–(C15) provide an indication of the quality of the coding of the program, they are not by themselves sufficient to provide a test of the convergence and accuracy of the method.

-
- [1] M. Hutley, *Diffraction Gratings* (Academic Press, New York, 1982).
- [2] E. Loewen and E. Popov, *Diffraction Gratings and Applications* (Dekker, New York, 1997).
- [3] J. P. Dowling, <http://home.earthlink.net/~jpdowling/pbgbib.html>
- [4] S. Y. Lin and J. G. Fleming, *IEEE J. Lightwave Technol.* **17**, 1944 (1999).
- [5] S. Y. Lin and J. G. Fleming, *Opt. Lett.* **24**, 49 (1999).
- [6] T. A. Birks, J. C. Knight, and P. S. J. Russell, *Opt. Lett.* **22**, 961 (1997).
- [7] T. M. Monro, D. J. Richardson, N. G. R. Broderick, and P. J. Bennett, *J. Lightwave Technol.* **17**, 1093 (2000).
- [8] T. A. Birks, P. J. Roberts, P. S. J. Russell, D. M. Atkin, and T. J. Shepherd, *Electron. Lett.* **31**, 1941 (1995).
- [9] J. C. Knight, J. Broeng, T. A. Birks, and P. S. J. Russell, *Science* **282**, 1476 (1998).
- [10] J. Broeng, T. Sondergaard, S. E. Barkou, P. M. Barbeito, and A. Bjarklev, *J. Opt. A, Pure Appl. Opt.* **1**, 477 (1999).
- [11] R. C. McPhedran, L. C. Botten, A. A. Asatryan, N. A. Nicorovici, C. M. de Sterke, and P. A. Robinson, *Aust. J. Phys.* **52**, 791 (1999).
- [12] R. C. McPhedran, L. C. Botten, A. A. Asatryan, N. A. Nicorovici, P. A. Robinson, and C. M. de Sterke, *Phys. Rev. E* **60**, 7614 (1999).
- [13] L. Li, *J. Opt. Soc. Am. A* **40**, 553 (1993).
- [14] L. C. Botten *et al.*, *Opt. Acta* **28**, 413 (1981); **28**, 1087 (1981).
- [15] E. Centeno and D. Felbacq, *J. Opt. Soc. Am.* **17**, 320 (2000).
- [16] D. Felbacq and E. Centeno, *Opt. Commun.* **199**, 39 (2001).
- [17] B. Gralak, Ph.D. thesis, Université Aix-Marseille, 2001.
- [18] L. C. Botten, N. A. Nicorovici, A. A. Asatryan, R. C. McPhedran, C. M. de Sterke, and P. A. Robinson, *J. Opt. Soc. Am. A* **17**, 2165 (2000).
- [19] L. C. Botten, N. A. Nicorovici, R. C. McPhedran, C. M. de Sterke, and A. A. Asatryan, *Phys. Rev. E* **64**, 046603 (2001).
- [20] *Electromagnetic Theory of Gratings*, edited by R. Petit, Topics in Current Physics Vol. 22 (Springer-Verlag, Berlin, 1980).
- [21] L. C. Botten, N. A. Nicorovici, A. A. Asatryan, R. C. McPhedran, C. M. de Sterke, and P. A. Robinson, *J. Opt. Soc. Am. A* **17**, 2177 (2000).

- [22] J. D. Joannopoulos, R. D. Meade, and J. N. Winn, *Photonic Crystals: Molding the Flow of Light* (Princeton University, New Jersey, 1995).
- [23] R. C. McPhedran, N. A. Nicorovici, and L. C. Botten, *J. Electromagn. Waves Appl.* **11**, 981 (1997).
- [24] J. W. Strutt, *Philos. Mag.* **34**, 481 (1892).
- [25] W. von Ignatowsky, *Ann. Phys. (Paris)* **44**, 369 (1914).
- [26] N. A. Nicorovici, R. C. McPhedran, and R. Petit, *Phys. Rev. E* **49**, 4563 (1994).
- [27] N. A. Nicorovici and R. C. McPhedran, *Phys. Rev. E* **50**, 3143 (1994).
- [28] E. G. McRae, *Surf. Sci.* **11**, 479 (1968); **11**, 492 (1968).
- [29] L. Li, *J. Opt. Soc. Am. A* **13**, 1024 (1996).
- [30] J. M. Elson and P. Tran, *J. Opt. Soc. Am. A* **12**, 1765 (1995).
- [31] T. P. White, R. McPhedran, L. Botten, G. Smith, and C. de Sterke, *Opt. Express* **9**, 721 (2001).
- [32] T. P. White, B. Kuhlmeiy, R. C. McPhedran, D. Maystre, G. Renversez, C. M. de Sterke, and L. C. Botten, *J. Opt. Soc. Am. B* **19**, 2322 (2002).
- [33] B. T. Kuhlmeiy, T. P. White, G. Renversez, D. Maystre, L. C. Botten, C. M. de Sterke, and R. C. McPhedran, *J. Opt. Soc. Am. B* **19**, 2331 (2002).
- [34] T. P. White, R. McPhedran, C. de Sterke, L. Botten, and M. Steel, *Opt. Lett.* **26**, 1660 (2001).
- [35] J. Broeng, S. E. Barkou, T. Sondergaard, and A. Bjarklev, *Opt. Lett.* **25**, 96 (2000).
- [36] V. Twersky, *Arch. Ration. Mech. Anal.* **8**, 323 (1961).
- [37] J. D. Jackson, *Classical Electrodynamics* (Wiley, New York, 1975).